Follow-on to the Inter-comparison of Satellite-based Volcanic Ash Retrieval Algorithms in Support to SCOPE-Nowcasting

Final report

Version 1.0

Prepared by

Gareth Thomas and Richard Siddans

RAL Space

Remote Sensing Group

Harwell Oxford

Didcot, OX11 0QX

United Kingdom

EUMETSAT Contract: EUM/C0/18/ 4600002135/RM

2019-03-21

CONTENTS

ACRONYMS USED IN THIS DOCUMENT

Table 1: List of acronyms used in this report

CALIOP	Cloud-Aerosol Lidar with Orthogonal Polarization
CALIPSO	Cloud-Aerosol Lidar and Infrared Pathfinder Satellite Observation
RAL	Rutherford Appleton Laboratory
RGB	Red-Green-Blue
RL	Lower Right (image coordinate)
SEVIRI	Spinning Enhanced Visible/Infrared Imager
UL	Upper Left (image coordinate)

1 INTRODUCTION

This document provides detailed findings of the study “Follow-on to the Inter-comparison of Satellite-based Volcanic Ash Retrieval Algorithms in Support to SCOPE-Nowcasting” (undertaken in response to the EUMETSAT RFQ 18/215736), under the auspices of the WMO SCOPE-Nowcasting Pilot Project 2: “Globally consistent Volcanic Ash Products”. This work follows on from, and extends, the study “Satellite Derived Volcanic Ash Product Inter-Comparison in Support of SCOPE-Nowcasting” undertaken in 2015-2016 and reported on in RD-3 and RD-XX. The overall aims of the SCOPE-Nowcasting activity were:

1. Using pre-selected cases, quantify the differences between satellite-derived volcanic ash cloud properties derived from different techniques and sensors.
2. Establish basic validation protocol for satellite-derived volcanic ash cloud properties.
3. Document the strengths and weaknesses of different remote sensing approaches as a function of satellite sensor.
4. Standardize the units and quality flags associated with volcanic cloud geophysical parameters.
5. Provide recommendations to Volcanic Ash Advisory Centers (VAACs) and other users on how to best to utilize quantitative satellite products in operations.
6. Create a "road map" for future volcanic ash related scientific developments and inter-comparison/validation activities that can also be applied to SO_2 clouds and emergent volcanic clouds.

As described in the statements of work (RD-2, RD-4), the aim of these studies was to perform the inter-comparison work needed to support the overall aims above, particularly addressing points 1, 2 and 4, with some initial findings on 3. The original study provided results for discussion at the “Intercomparison of Satellite-based Volcanic Ash Retrieval Algorithms with WMO SCOPE-Nowcasting” workshop, which was held in Madison, WI, USA from 29 June – 2 July 2015. Findings of the workshop are given in RD-3. Likewise, the current work provided results for the “Second Meeting on the Inter-comparison of Satellite-based Volcanic Ash Retrieval Algorithms within WMO SCOPE-Nowcasting”, held in Catania, Italy from 8 – 12 October 2018.

This study extends on the previous work in two main ways:

1. New satellite ash products are included in the inter-comparison, including from the Advanced Himawari Imager (AHI) instrument, and new versions of many of the products supplied in the first intercomparison have been updated.
2. The intercomparison has been extended, primarily by partitioning the intercomparison according to viewing conditions and geometry.

2 BACKGROUND

The Intercomparison of Satellite-based Volcanic Ash Retrieval Algorithms with WMO SCOPE-Nowcasting activity (hence forth referred to the SCOPE-ash) is motivated by the need to ensure that high quality volcanic ash products are available to improve the ash advisories provided to aviation users. There has been significant evolution in the quantitative remote sensing of volcanic ash clouds by satellite over the past decade, and especially since the costly disruption to aviation caused by the Eyjafjallajökull eruption in 2010. There now exist a plethora of different ash products from a wide range of satellite sensors and employing diverse approaches to the characterisation of ash. Although most of these products have been individually assessed, and there have been some limited inter-comparison exercises, the original 2015/16 SCOPE-ash project was the first attempt to perform a comprehensive inter-comparison and assessment of satellite ash retrievals. This follow-on project aims to revisit the first study in the light of the findings of that work, developments in algorithms and the availability of new sensors.

SCOPE-ash also represented the first attempt to define standards for the geophysical parameters, and their representation, in satellite ash products and a validation approach for satellite volcanic ash products. The results of both studies, combined with the discussions of satellite retrieval experts and VAAC representatives at the associated workshops, will be used to help VAACs and other users better utilise satellite based ash products, with the aim of improving the accuracy of volcanic ash advisories.

The data format specification provided for SCOPE-ash was included in the project Work Plan, and was based on that developed for the EUMETSAT project “Development of OCA type processors to volcanic ash detection and retrieval” (RD-1). Products formatted according to this specification were uploaded directly to a password protected FTP repository supplied by RAL Space. These data were then processed through the inter-comparison software developed during the previous study, producing a large number of plots and summary statistics. These were, in turn, made available to the SCOPE-ash organizing committee and data contributors ahead of the Madision workshop, at which the inter-comparison was discussed in the context of the six objectives listed above.

3 STUDY CASES

The volcanic eruption study cases used in the inter-comparison exercise were defined in the Work Plan and are summarised in Table 2, while the satellite products submitted for the inter-comparison are listed in Table 3. The exact scenes to include in the study varied by satellite and instrument, depending on the spatial and temporal coverage provided by each. A summary of the number of data files provided for each day of each eruption case, for each product included in the inter-comparison is given in Figure 1.

Eruption	Date range	Comment
Eyjafjallajökull	2010-04-16 – 2010-05-18	Included in previous study
Grimsvötn	2011-05-21 – 2011-05-23	Included in previous study
Puyehue-Cordon Caulle	2011-06-05 – 2011-06-18	Included in previous study
Rinjani	2015-11-04	Newly added
Etna	2015-12-04	Newly added

Table 2: Eruption cases used in this study, including three which were also used in the original study and two which were selected to cater to products utilising the Himawari platform.

	20100416 EYJAFJALLAJOKULL	20100505 EYJAFJALLAJOKULL	20100506 EYJAFJALLAJOKULL	20100507 EYJAFJALLAJOKULL	20100508 EYJAFJALLAJOKULL	20100509 EYJAFJALLAJOKULL	20100510 EYJAFJALLAJOKULL	20100511 EYJAFJALLAJOKULL	20100512 EYJAFJALLAJOKULL	20100513 EYJAFJALLAJOKULL	20100514 EYJAFJALLAJOKULL	20100516 EYJAFJALLAJOKULL	20100517 EYJAFJALLAJOKULL	20100518 EYJAFJALLAJOKULL	20110521 GRIMSVOTN	20110522 GRIMSVOTN	20110523 GRIMSVOTN	20110605 PUYEHUE	20110615 PUYEHUE	20110616 PUYEHUE	20110617 PUYEHUE	20110618 PUYEHUE	20151104 RINJANI	20151204 ETNA
CALIPSO_RAL		1	1	2	3	2	2	1	3	1	2	1	2	2		1	3	2	1	7	5	1		
CALIOP	1															1	1	1	2	5	5	3		
EARLINET_IMAA	20																							
SEVIRI_MANUAL2		1	1	1	1	1	1	1	1	1	1	1	1	1	8	10	2							17
SEVIRI_MANUAL1		1	1	1	1	1	1	1	1	1	1	1	1	1	8	10	2							17
HIMAWARI8_MANUAL2																							11	
HIMAWARI8_MANUAL1																							11	
MISR_RA				1																				
TERRA_MODIS_RAL	48											45					45							
TERRA_MODIS_ORAC	11	4	3	6	7	7	8	9	8	11	9	10	8	11	1					8				
SEVIRI_VPR																								53
SEVIRI_VOLCAT					1																			
SEVIRI_VADUGS	40	20	1	2	3	1									8	37	3	2	3	48	8	5		
SEVIRI_ORAC_RAL	1		1	2	2	3	1	1	1	2	2	2	2			1	2	2	1	8	5	2		
SEVIRI_NOAA	40	21	1	2	3	17	2	1	1	13	27	21	33	24	8	37	3							60
SEVIRI_MO	40	21	1	2	3	17	2	1	1	13	27	21	33	24	8	37	3	2	3	48	8	5		60
SEVIRI_EUMOP	40	21	1	2	3	16	2	1	1	13	21	21	32	24	8	37	3	2	3	47	8	5		
SEVIRI_CMA	94	22	1	2	3	17	2	1	1	13	2	21	33	29				2	2	9				
MODIS_VPR	19	8	7	12	15	15	17	16	19	19	20	18	19	20										2
MODIS_NOAA	9	4	3	6	8	7	8	9	11	10	10	9	11	10		2	2		2	9	6	2		
MODIS_MO	20	8	7	12	15	15	16	17	19	21	18	20	20	19	1	2	2	1	2	18	5	3	1	3
MODIS_LUT	19	8	7	12	15	15	17	16	19	19	20	18	19	20										
MODIS_CENIZARG																		1		4				
MISR_NASA				1		1	1		1			1		1		1								1
METOPA_PMA	7	4	4	6	8	8	7	8	10	10	11	12	10	9						8				4
IASI_ULB	9	4	4	6	8	8	7	7	10	8	10	9	10	9										
IASI_OXFORD															6	8	10			14				
IASI_MO	9	4	4	6	8	8	8	8	10	8	11	10	10	10	1					8			1	4
HIMAWARI8_NOAA																							11	
HIMAWARI8_MSNZ																							11	
BRISTOL_SEVIRI	33	17	1	2	3	17	2	1	1	13	27	21	33	29				2	3	47	5			6
BRISTOL_IASI			2																					
BOM_VOLCAT																							10	
AVHRR_PLANETA	2		2	2	2	1	2	2	3	3	2	3	3	3	1					2				2
AVHRR_MO	8	4	4	6	8	8	7	7	10	10	11	9	10	10	1					8				
AQUA_MODIS_RAL	39											45					34							
AQUA_MODIS_ORAC	10	4	4	6	7	7	8	7	10	10	10	7	11	10		1	2	1	2	8	5	3		
AHI_VADUGS																							11	
AHI_MO																							11	
AATSR_FMI	2		2	1	1	2	2	1	2	1	2	2	1	1		1	1	1						

	em_10	em_550	cth	r_eff	mass
CALIPSO_RAL			■		
CALIOP		■	■		■
EARLINET_IMAA			■		
SEVIRI_MANUAL2					
SEVIRI_MANUAL1					
HIMAWARI8_MANUAL2					
HIMAWARI8_MANUAL1					
MISR_RA		■	■	■	
TERRA_MODIS_RAL		■	■	■	■
TERRA_MODIS_ORAC	■	■	■	■	■
SEVIRI_VPR	■	■	■	■	■
SEVIRI_VOLCAT					
SEVIRI_VADUGS			■	■	■
SEVIRI_ORAC_RAL	■	■	■	■	■
SEVIRI_NOAA	■		■	■	■
SEVIRI_MO	■	■	■	■	■
SEVIRI_EUMOP	■		■	■	■
SEVIRI_CMA			■	■	
MODIS_VPR	■	■	■	■	■
MODIS_NOAA	■		■	■	■
MODIS_MO	■	■	■	■	■
MODIS_LUT	■	■	■	■	■
MODIS_CENIZARG	■			■	■
MISR_NASA			■		
METOPA_PMA		■			
IASI_ULB	■			■	■
IASI_OXFORD	■	■	■	■	■
IASI_MO	■	■	■	■	■
HIMAWARI8_NOAA	■		■	■	■
HIMAWARI8_MSNZ	■		■	■	■
BRISTOL_SEVIRI			■	■	■
BRISTOL_IASI			■	■	■
BOM_VOLCAT	■		■	■	■
AVHRR_PLANETA	■	■	■	■	■
AVHRR_MO	■	■	■	■	■
AQUA_MODIS_RAL		■	■	■	■
AQUA_MODIS_ORAC	■	■	■	■	■
AHI_VADUGS			■	■	■
AHI_MO	■	■	■	■	■
AATSR_FMI		■	■	■	■

Figure 1: Overview of the data files provided by comparison product for study case day. The green boxes on the right indicate which ash properties are provided by each product. The products tinted grey are those considered to be validation data for the study. Figures in each box give the number of files provided in each case (and the colour-code reflects this). It should be noted that the number of files should not be taken as an indicator of the data volume or coverage as this depends also on the granularity of the products (chosen by the provider, usually following the granularity of the instrument L1 data). The statistic served during the project to cross-check that the correct number of files had been received and processed at RAL. The main purpose of the table here is to indicate which eruptions were covered by which sensor and which products are provided.

Product identifier	**Source institution**	**Contact person**	**Comments**
CALIPSO_RAL	NASA/RAL	Charles Trepte (NASA) charles.r.trepte@nasa.gov Richard Siddans richard.siddans@stfc.ac.uk	Regridded CALIOP level 1b attenuated backscatter. Used for height validation.
MISR_RA	NASA	Ralph Kahn ralph.kahn@nasa.gov Jim Limbacher jim.limbacher@nasa.gov	Stereo-parallax based ash height retrieval. Used for height validation. *Same data as used previously*
FAAM_MO	UK Met Office	Franco Marenco franco.marenco@metoffice.co.uk	Extinction data from the Leosphere ALS450 lidar system on board the NERC FAAM aircraft. Used for height validation. *Same data as used previously*
EARLINET_IMAA	Various	Gelsomina Pappalardo Gelsomina.pappalardo@imaa.cnr.it	Ground based lidar measurements. Used for height validation. *Same data as used previously*
HIMAWARI8_MANUAL1	National Oceanic and Atmospheric Administration (NOAA)	Mike Pavolonis michael.pavolonis@nasa.gov	Expert classified Himawari-8 AHI scenes. Used for evaluating ash detection.
HIMAWARI8_MANUAL2	National Oceanic and Atmospheric Administration (NOAA)	Mike Pavolonis michael.pavolonis@nasa.gov	Expert classified Himawari-8 AHI scenes. Used for evaluating ash detection.
SEVIRI_MANUAL1	National Oceanic and Atmospheric Administration (NOAA)	Mike Pavolonis michael.pavolonis@nasa.gov	Expert classified SEVIRI scenes. Used for evaluating ash detection.
SEVIRI_MANUAL2	National Oceanic and Atmospheric Administration (NOAA)	Mike Pavolonis michael.pavolonis@nasa.gov	Expert classified SEVIRI scenes. Used for evaluating ash detection.
SEVIRI_VOLCAT	National Oceanic and Atmospheric Administration (NOAA)	Mike Pavolonis michael.pavolonis@nasa.gov	Expert classified SEVIRI scene. Used for evaluating ash detection. *Same data as used previously*
AATSR_FMI	Finnish Meteorological Institute (FMI)	Timo Virtanen timo.h.virtanen@fmi.fi	Stereo-parallax ash height retrieval. *Same data as used previously*
AHI_MO	UK Met Office	Mike Cooke Michael.c.cooke@metoffice.gov.uk	
AHI_VADUGS	Deutsches Zentrum für Luft- and Raumfahrt (DLR)	Margarita Vazquez margarita.vazquez@dlr.de	
AVHRR_MO	UK Met Office	Pete Francis pete.francis@metoffice.gov.uk Mike Cooke michael.cooke@metoffice.gov.uk	*Same data as used previously*
AVHRR_PLANETA	SRC PLANETA (Moscow)	Andrei Filei andreyvm-61@mail.ru	
BOM_VOLCAT	Australian Bureau of Meteorology	Chris Lucas chris.lucas@bom.gov.au	Himawari-8 AHI product
BRISTOL_IASI	University of Bristol	Luke Western luke.western@bristol.ac.uk	*Same data as used previously*
BRISTOL_SEVIRI	University of Bristol	Luke Western luke.western@bristol.ac.uk	

HIMAWARI8_MSNZ	New Zealand MetService	Cory Davis cory.davis@metservice.com	
HIMAWARI8_NOAA	National Oceanic and Atmospheric Administration (NOAA)	Mike Pavolonis mike.pavolonis@noaa.gov	
IASI_MO	UK MetOffice	Mike Cooke michael.c.cooke@metoffice.gov.uk	
IASI_OXFORD	University of Oxford	Lucy Ventress ventress@atm.ox.ac.uk	
IASI_ULB	Université Libre de Brusselles (ULB)	Lieven Clarisse lieven.clarisse@ulb.ac.be	*Same data as used previously*
METOPA_PMA	EUMETSAT	Ruediger Lang ruediger.lang@eumetsat.int	Combined GOME-2/AVHRR product.
MODIS_BOM	Australian Bureau of Meteorology (BOM)	Chris Lucas c.lucas@bom.gov.au	*Same data as used previously*
MODIS_CENIZARG	Argentine National Commission for Space Activities (CONAE)	Guillermo Toyos gtoyos@conae.gov.ar	*Same data as used previously*
MODIS_LUT	Italian Istituto Nazionale di Geofisica e Vulcanologia (INGV)	Stefano Corradini stefano.corradini@ingv.it Luca Merucci luca.meruci@ingv.it	*Same data as used previously*
MODIS_MO	UK MetOffice	Mike Cooke michael.c.cooke@metoffice.gov.uk	
MODIS_NOAA	National Oceanic and Atmospheric Administration (NOAA)	Mike Pavolonis mike.pavolonis@noaa.gov	*Same data as used previously*

Product identifier	**Source institution**	**Contact person**	**Comments**
TERRA/AQUA_MODIS_ORAC	University of Oxford	Greg McGarragh g.mcgarragh1@physics.ox.ac.uk	*Same data as used previously*
TERRA/AQUA_MODIS_RAL	RAL Space	Richard Siddans richard.siddans@stfc.ac.uk	*Same data as used previously*
MODIS_VPR	Italian Istituto Nazionale di Geofisica e Vulcanologia (INGV)	Stefano Corradini stefano.corradini@ingv.it Luca Merucci luca.meruci@ingv.it	*Same data as used previously*
MTSAT1R_JMA	Japanese Meteorological Agency (JMA)	Daisaku Uesawa d-uesawa@met.kishou.go.jp	*Same data as used previously*
MTSAT2_JMA	Japanese Meteorological Agency (JMA)	Daisaku Uesawa d-uesawa@met.kishou.go.jp	*Same data as used previously*
MTSAT2_BOM	Australian Bureau of Meteorology (BOM)	Chris Lucas c.lucas@bom.gov.au	*Same data as used previously*
SEVIRI_CMA	China Meteorological	Lin Zhu zhulin@cma.gov.cn	

	Administration (CMA)		
SEVIRI_EUMOP	EUMETSAT	Hans-Joachim Lutz hansjoachim.lutz@eumetsat.int	*Same data as used previously*
SEVIRI_MO	UK Met Office	Pete Francis pete.francis@metoffice.gov.uk Mike Cooke michael.cooke@metoffice.gov.uk	
SEVIRI_NOAA	National Oceanic and Atmospheric Administration (NOAA)	Mike Pavolonis mike.pavolonis@noaa.gov	
SEVIRI_ORAC_RAL	RAL Space	Richard Siddans richard.siddans@stfc.ac.uk Gareth Thomas gareth.thomas@stfc.ac.uk	*Same data as used previously*
SEVIRI_VADUGS	Deutsches Zentrum für Luft- and Raumfahrt (DLR)	Kaspar Graf kaspar.graf@dlr.de	*Same data as used previously*
SEVIRI_VPR	Italian Istituto Nazionale di Geofisica e Vulcanologia (INGV)	Riccardo Biondi, Stefano Corradini, Luca Merucci, Lorenzo Guerrieri riccardo@biondiriccardo.it, stefano.corradini@ingv.it, luca.merucci@ingv.it, lorenzo.guerrieri@unimore.it	

Table 3: Key to data products included in this study.

4 INTERCOMPARISON APPROACH

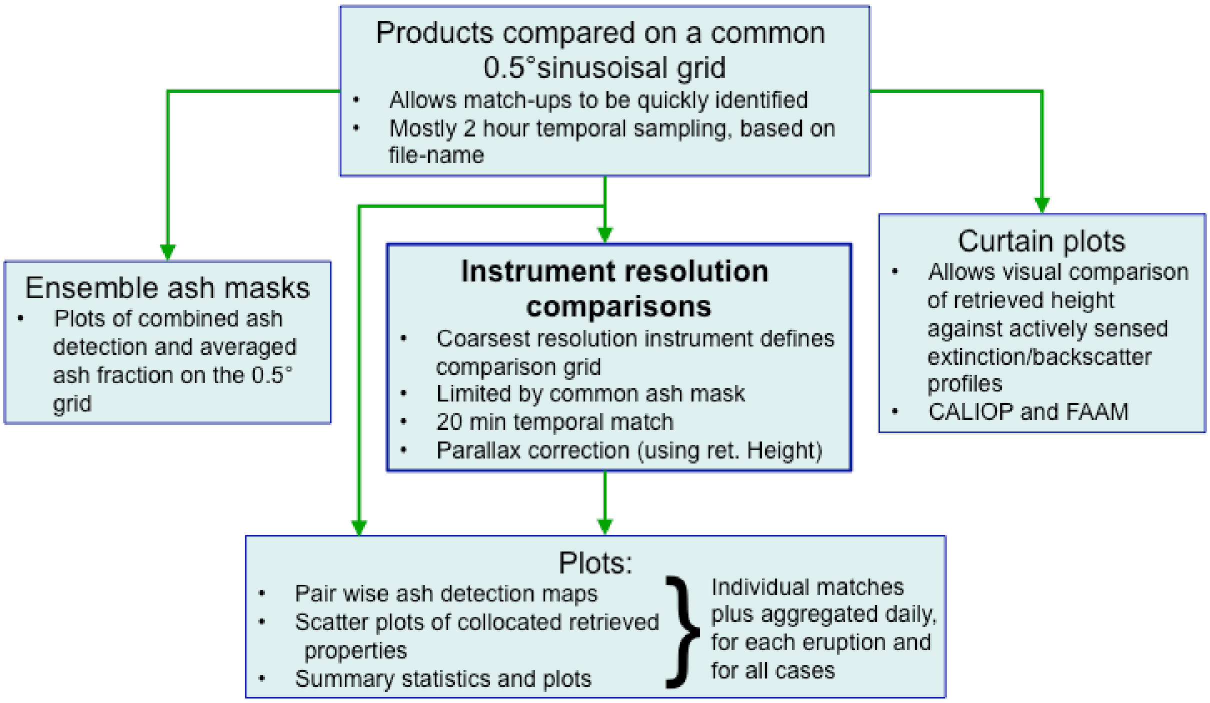

Figure 2: Overview of the intercomparison methodology.

The SCOPE-ash study involved the comparison of products from instruments with a wide range of spatial resolutions and spectral sensitivity, as well as an equally wide range of algorithm approaches. The "fair" comparison of all of these products is thus not straightforward. The approach taken in the study was to use a hierarchy of comparisons at different spatial and temporal resolutions, starting with a "lowest common denominator" 0.5° sinusoidal grid with a lower resolution than any included product, and working up to pixel-by-pixel comparisons at instrument resolution for products from the same sensor. The comparison methodology is summarised in Figure 1 and is given in more detail in the following sections.

All plots produced in the intercomparison are automatically organised into a file-structure, which is online via password protected FTP: ftp://ftp.rsg.rl.ac.uk/ with the user-name "scopeftp" and password "Sc0pe2015(Eve23)". Table 4 provides details of the locations of the plots described in the following sections.

Directory	Reference	Description
reprojected_pngs/cv0p1/no_parallax_0p5deg	Section 4.1	Maps of the regridded products on the 0.5° grid.
reprojected_pngs/cv0p1/inst_res	Section 4.1	Maps of the products regridded to the instrument resolution grids. There is one image of each scene for each instrument grid used (see Section 4.6)
matches_pngs		Contains all the pair-wise comparison plots in a series of sub-folders:

matches_pngs/mv0p1-iza_0-30		Contains comparison plots filtered so that only pixels with the indicated range of instrument zenith angle.
matches_pngs/mv0p1-ocean or -land		Contains comparison plots filtered so that only pixels over ocean or land, respectively.
matches_pngs/mv0p1-filterSEVIRI_NOAA	Section 4.2	Contains comparison plots filtered so that only pixels flagged as ash by the SEVIRI-NOAA product are included.
matches_pngs/mv0p1-filterSEVIRI_MANUAL1 matches_pngs/mv0p1-filterSEVIRI_MANUAL2 matches_pngs/mv0p1-filterHIMAWARI8_MANUAL1 matches_pngs/mv0p1-filterHIMAWARI8_MANUAL2	Section 6.2	Contains comparison plots filtered so that only pixels flagged as ash by the corresponding manually classified product are included
matches_pngs/mv0p1-filterSEVIRI_NOAA-min_em=0p05	Section 4.2	Contains comparison plots filtered so that only pixels flagged as ash by the SEVIRI-NOAA product and for which the emissivity at 10 µm is greater than 0.05 are included.
matches_pngs/mv0p1-filterSEVIRI_NOAA-min_em=0p1	Section 4.2	Contains comparison plots filtered so that only pixels flagged as ash by the SEVIRI-NOAA product and for which the emissivity at 10 µm is greater than 0.1 are included.
matches_pngs/mv0p1-min_em=0p05	Section 4.2	Contains comparison plots filtered so that only pixels for which the emissivity at 10 µm is greater than 0.05 are included.
matches_pngs/mv0p1-min_em=0p1	Section 4.2	Contains comparison plots filtered so that only pixels for which the emissivity at 10 µm is greater than 0.1 are included.
matches_pngs/*/no_parallax_0p5deg	Section 4.2	Sub-directory of each of the mv0p1 folders: contains the comparisons on the 0.5° sinusoidal grid.
matches_pngs/*/no_parallax_inst_res	Section 4.6	Sub-directory of each of the mv0p1 folders: contains the instrument resolution comparisons without parallax correction.
matches_pngs/*/inst_res	Section 4.6	Sub-directory of each of the mv0p1 folders: contains the instrument resolution comparisons including parallax correction.
ensemble_mask_pngs/cv0p1	Section 4.3	Contains the ensemble ash mask plots
calipso_curtain_pngs/mv0p1	Section 4.4	Contains the comparison plots against the CALIOP attenuated backscatter profile.
faam_curtain_pngs/mv0p1	Section 4.4	Contains the comparison plots against the FAAM aircraft lidar extinction profile.

Table 4: Overview of the directory structure used for the comparison plots.

4.1 PRODUCT REGRIDDING

The initial step in performing the inter-comparison is to pre-process all products, averaging each onto a 0.5° sinusoidal grid defined on an eruption-by-eruption basis. The grid for each eruption is defined such that its central point is located at the centre of the region defined for each eruption, which ensures that the grid cells are close to square boxes on the Earth's surface (the grid cells of a sinusoidal grid become increasingly skewed quadrilaterals on the surface as one approaches the edge of the grid).

This gridding was performed not only on the products evaluated in the study, but also on the validation data sets; namely CALIOP and FAAM lidar profiles, EARLINET ground based lidars and the expert classified SEVIRI scene. These products are thus included in the 0.5° and instrument resolution comparisons described below.

In order to minimise the influence of the different instrument resolutions and differences in the fraction of detected ash in each grid cell between products, the averaging of retrieved ash properties is weighted:

- Ash optical depth are converted to "emissivity", defined as:
$$\varepsilon_\lambda = 1.0 - \exp(-\tau_\lambda) \qquad 1$$
where τ_λ is the optical depth at wavelength λ.
- Ash cloud-top height and effective radius are averaged weighted by the emissivity at 10 µm or, if the product does not include a 10 µm optical depth, the 550 nm emissivity. If optical depth is not defined at either wavelength, an unweighted mean is calculated.
- The unweighted ash column mass density is calculated, including pixels with no ash (i.e. zero mass).

4.2 PAIR-WISE COMPARISONS AT 0.5°

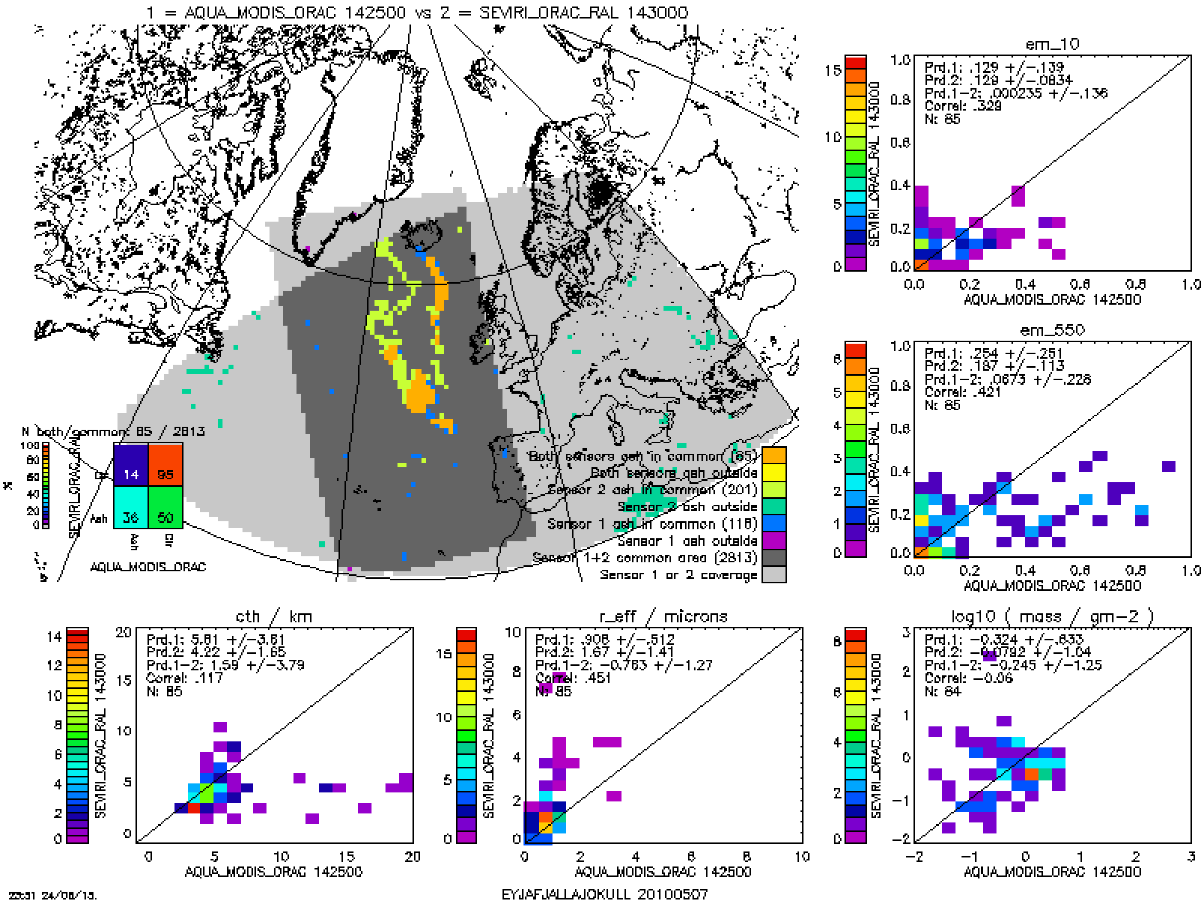

Figure 3: An example of a pair-wise comparison on the 0.5 grid, between the MODIS-AQUA ORAC product from University of Oxford and the SEVIRI ORAC product from RAL, for Eyjafjallajöjull at approximately 14:30 on 7 May 2010. In the map panel, the common area of the two products appears as dark grey, while grid cells containing ash in both products are coloured orange. Grid cells containing ash in the SEVIRI product within the overlap area but not detected as ash by the MODIS product are lime-green, while those detected by MODIS and not SEVIRI are blue.

Once regridded, each product pair was compared, using a ±1 hour temporal match criteria based on the time specified in the product file name (i.e. temporal matching of 0.5° gridded products did not require each file to be read, just a list of file names). From these matches, a series of plots were generated (see Figure 3):

- Pair-wise detection maps, and associated confusion matrices (top left panel of Figure 3), showing where each product pair agrees/disagrees on the presence of ash and the number of pixels:
  - Where both products have detected ash
  - Where both products are present, but only one has detected ash
  - Where both products are present and neither has detected ash
  - Where only one product is present and has, or has not, detected ash
- Scatter density plots of retrieved ash properties (for grid cells where both products detect ash): ash emissivity (as defined above) at 550 nm and 10 µm, ash cloud top height, ash effective radius and column ash mass density. Each of these includes associated statistics: mean and standard deviation of

each product, mean and standard deviation of the pixel-wise difference between each product, and Pearson correlation coefficient of the two products. Note that the plots actually included in each pairwise match, as shown in Figure 3, depends on the data fields provided by each product. In the case of match including a product that only provides an ash-detection mask, for instance, only the detection map and confusion matrix plots would be available.

The confusion matrices produced for each product pair provide a quantitative visual indication of the level agreement in ash detection as summarised in Table 5.

% of grid points where: $\left[\frac{\text{Sensor "Y" says clear}}{\text{Either sensor detects ash}}\right]$	% of grid points where: $\left[\frac{\text{Both sensors say clear}}{\text{Either sensor says clear}}\right]$
% of grid points where: $\left[\frac{\text{Both sensors detect ash}}{\text{Either sensor detects ash}}\right]$	% of grid points where: $\left[\frac{\text{Sensor "X" says clear}}{\text{Either sensor detects ash}}\right]$

Ideally	
0	100
100	0

Table 5: Description of ash detection confusion matrices, with an example of the ideal confusion matrix. Note that the confusion matrix is limited to the region where both satellite products provide coverage (e.g. the area shaded dark-grey in Figure 3).

In addition to plotting each individual temporal matchup, equivalent plots as also produced for aggregated matches on a daily basis, as well as across all matches found for a particular eruption. In addition, maps of the aggregated retrieval products for common pixels between the product pair are also plotted on a daily basis and for the whole eruption, as shown in Figure 4.

This analysis was also repeated limiting to pixels over land or ocean, or limiting to ranges of instrument viewing zenith angles (where products provide this information), as defined in Table 6

Directory	Description
matches_pngs/mv0p1-land	Matches over land only
matches_pngs/mv0p1-sea	Matches over sea only
matches_pngs/mv0p1_0-30	Matches limited to instrument zenith angle 0 – 30° in both products.
matches_pngs/mv0p1_30-60	As above, but for instrument zenith 30 – 60°

Table 6: Land/sea and instrument zenith angle limited matches

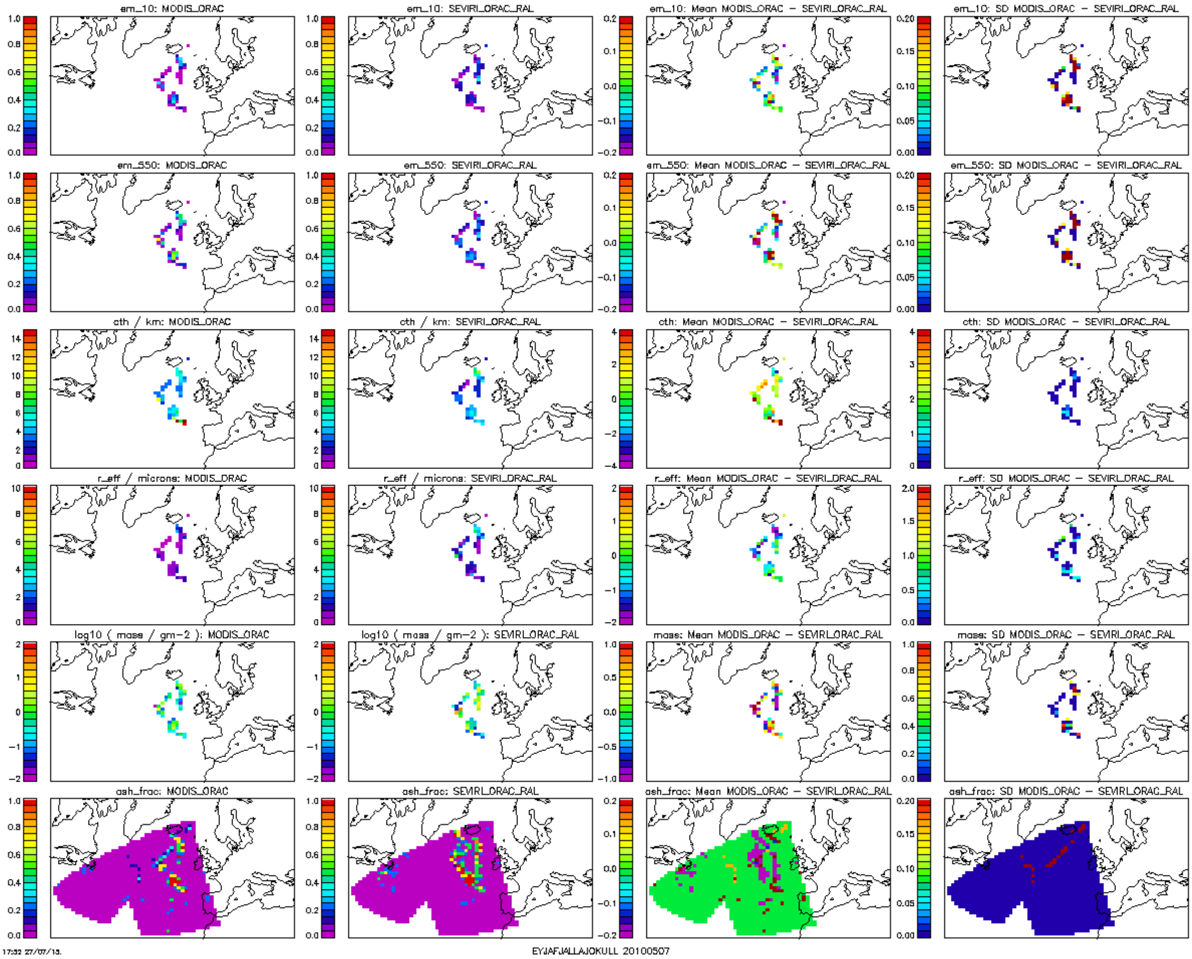

Figure 4: The daily summary maps for the same product pair as shown in Figure 3, on the same date.

Finally, the individual comparisons were combined into summary tables including all products for each eruption, both on a daily basis and for the entire eruption case. These tables include:

- Confusion matrices for all product pairs
- Detection maps
- Scatter plots of each retrieval parameter (ash cloud-top height, emissivity at 550 nm and 10 µm, effective radius and column mass density), along with the PDF of each parameter derived from each individual product, as shown in Figure 5.
- Matrix plots of the comparison statistics for each product pair (products X and Y) for ash detection (Figure 6):
    - Percentage miss-matched detection: number of ash pixels only detected in X / Number of ash pixels in X or Y.
    - Percentage consistent detection: number of ash pixels in X and Y / Number of ash pixels in X or Y (percentage)
    - The common ash cloud area detected by X and (X or Y)
    - The common ash cloud area detection by (X and Y) and (X or Y)

- Matrix plots of the comparison statistics for each product pair (products X and Y) for the retrieved parameters (Figure 1):
  - The mean difference (X – Y)
  - Standard deviation of the difference
  - Pearson correlation
  - Number of matching points

In addition to the basic comparison, where each product is compared as-is, comparisons have also been performed with additional constraints applied to the data:

- The manually classified SEVIRI and HIMAWARI scenes, provided in the HIMIWARI8_MANUAL1, HIMIWARI8_MANUAL2, SEVIRI_MANUAL1 and SEVIRI_MANUAL2, have been used to provide master ash flags, so that only pixels which have been manually classified as ash are included in the comparisons. Generally speaking the manual classifications are not notably more or less conservative than the automatic classification schemes, but do not suffer from the scattered false-positive ash detections displayed by many products. Thus, these comparisons effectively reduce the impact of such scattered false detections, allowing only pixels where ash is likely to be present to be compared.
- The same procedure has been performed using the NOAA SEVIRI product as the master ash-detection. This analysis was performed in the original 2015 SCOPE intercomparison, as only the single manually classified scene was available at that time, and the NOAA ash detection scheme shows a low rate of obvious false-positives. The analysis has been repeated in the new intercomparison to allow direct comparison to previous results.
- The data has been filtered by setting minimum value thresholds on the ash emissivity at 10 µm. This excludes optically thin ash from the comparisons, which can be expected to provide poorly constrained retrievals of ash properties, with sensitivity to underlying water cloud being a particular example. Emissivity thresholds of 0.1 and 0.05 have been used (which essentially correspond one-to-one with the 10 µm optical depth at these low values).
- The data has been segregated on the basis of whether pixels lie over land or ocean. The homogeneity of the ocean surface generally results in a lower false-positive detection rate in most schemes, as well as providing better constrained retrievals of ash properties.
- Data has also been segregated in terms of satellite instrument zenith angle, in an attempt to reveal any dependence on viewing geometry in the different products. Zenith angle ranges of < 30°, 30 – 60° and > 60° have been used.

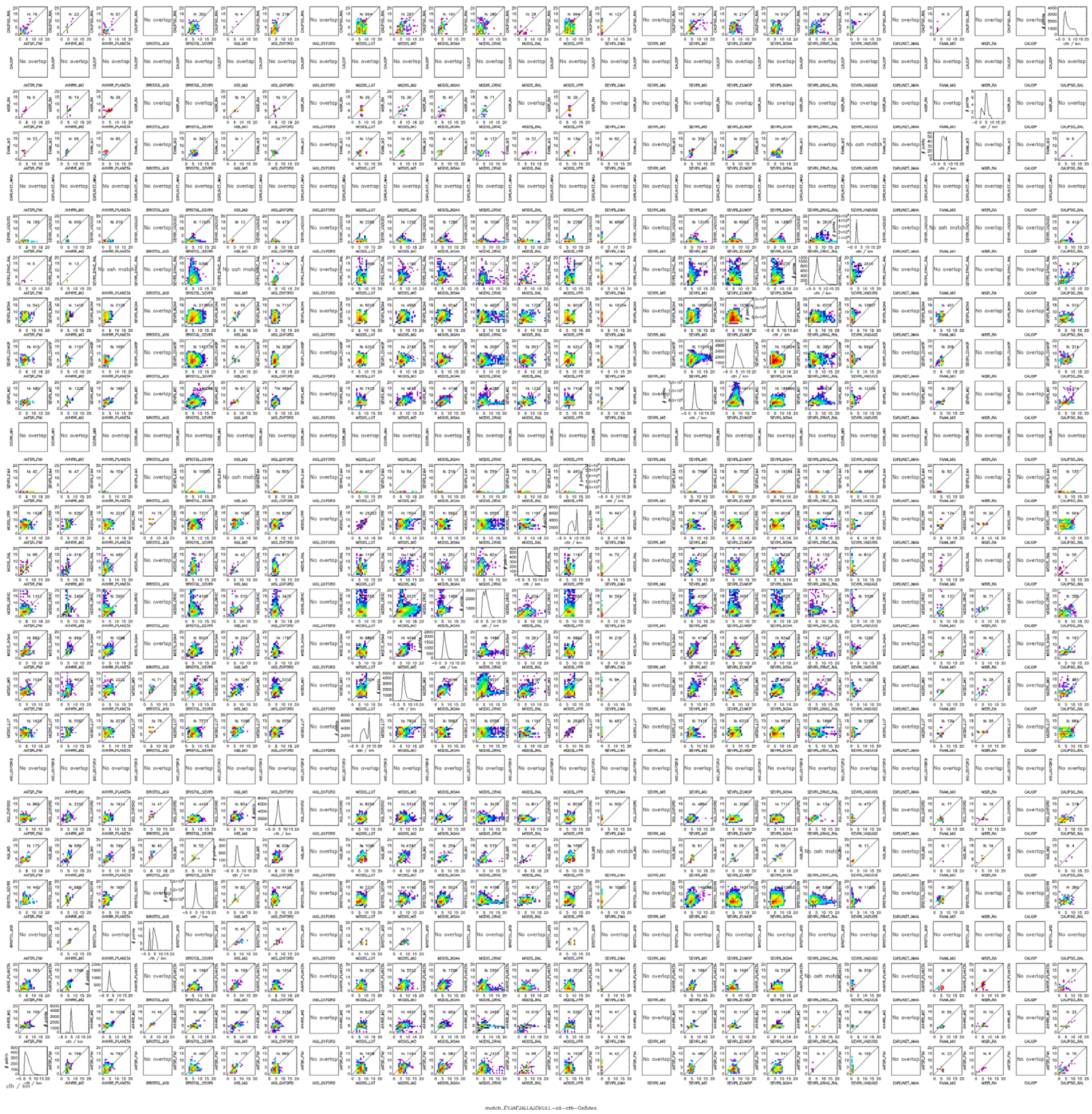

Figure 5: Summary plot table of ash cloud-top height comparisons for the Eyjafjallajökull eruption. Each panel shows the scatter plot for a product pair, with the PDF of ash cloud-top height for each product appearing along the diagonal. A full sized version of this plot can be accessed at the URL: scopeftp@ftp.rsg.rl.ac.uk/matches_pngs/mv0p1/no_parallax_0p5deg/00_overview/EYJAFJALLAJOKULL/all/match_EYJAFJALLAJOKULL-all-cth-0p5deg.png

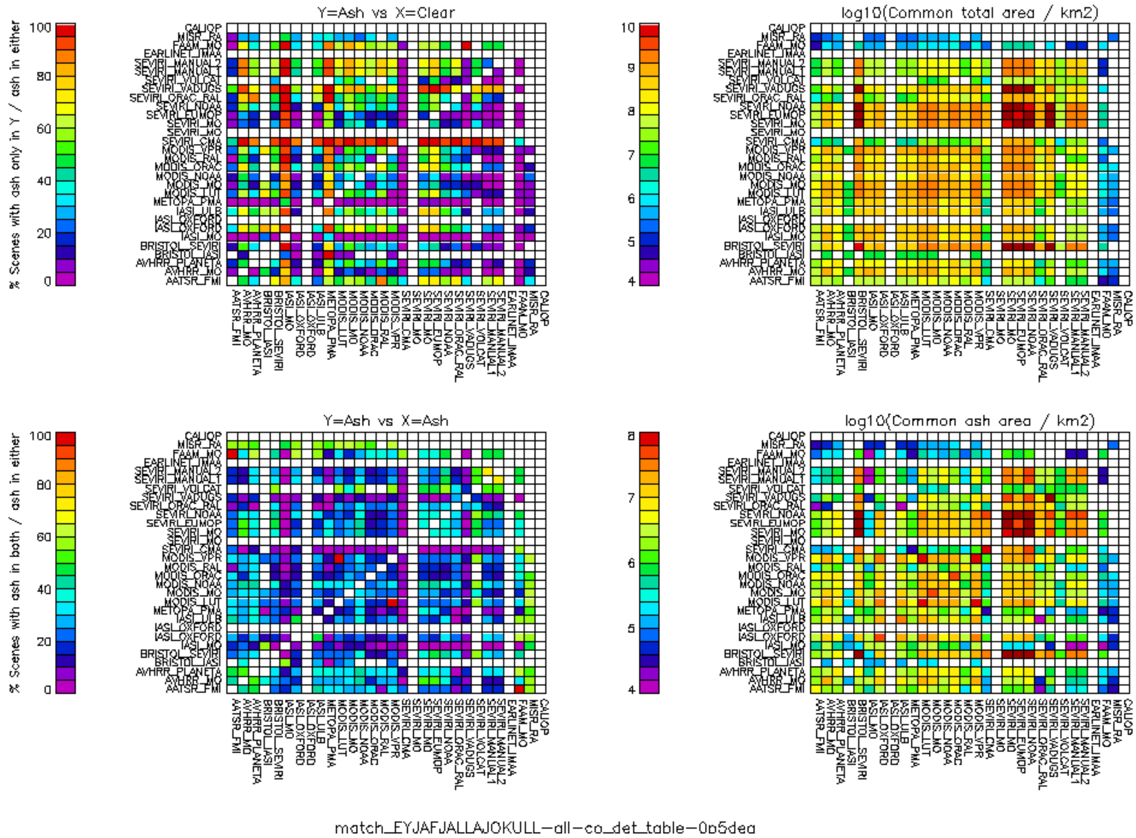

Figure 6: Statistics of the ash detection comparison for the Eyjafjallajökull eruption on the 0.5° grid. Clockwise from the top-left the panels show the percentage miss-matched ash detection between product pairs; the common area detected in product Y and (Y or X); the percentage consistent detection; the common area detected by products (Y and X) and (Y or X).

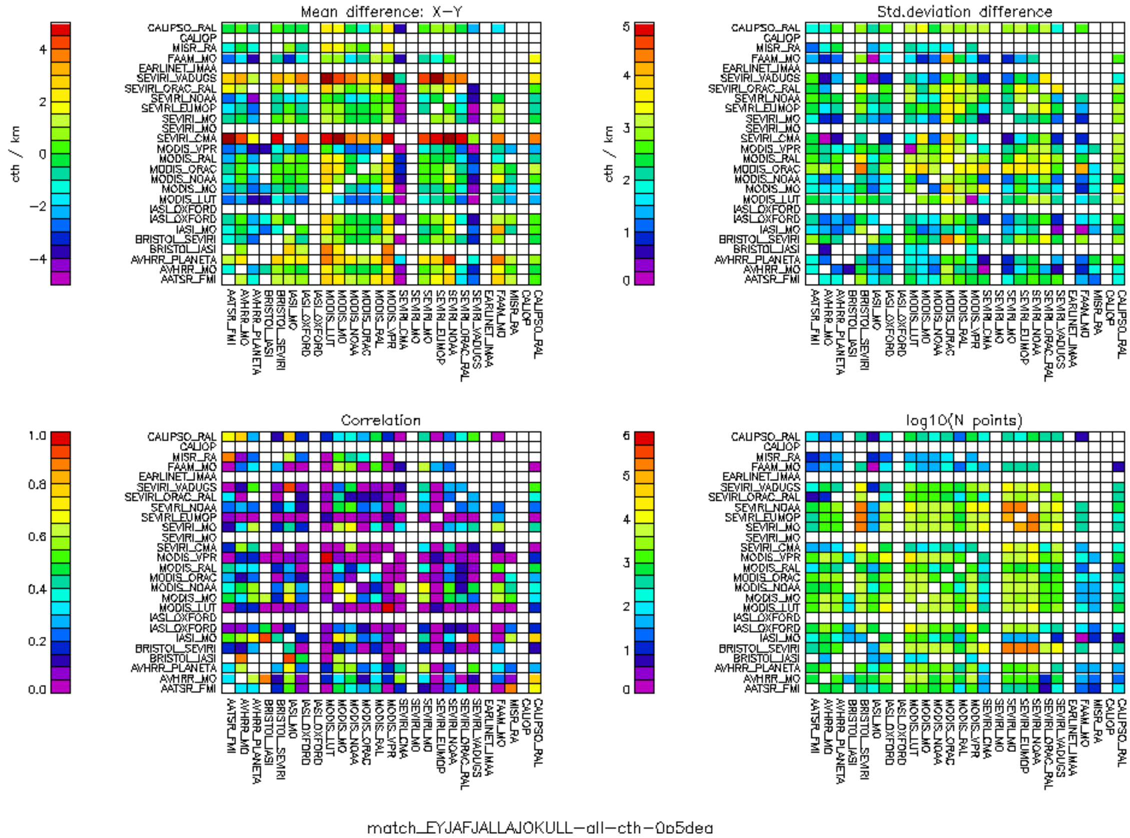

Figure 7: Summary statistics of the ash cloud-top height comparisons for the Eyjafjallajkull eruption, on the 0.5° grid.

4.3 ENSEMBLE ASH DETECTION MAPS

Using the matches defined above, ensemble ash detection maps were also produced, as shown in Figure 8. These plots show the number of products which provide data for each 0.5° grid cell and how many detected ash over a two hour window, as well as the average ash fraction (i.e. fraction of instrument pixels detected as ash within each 0.5°).

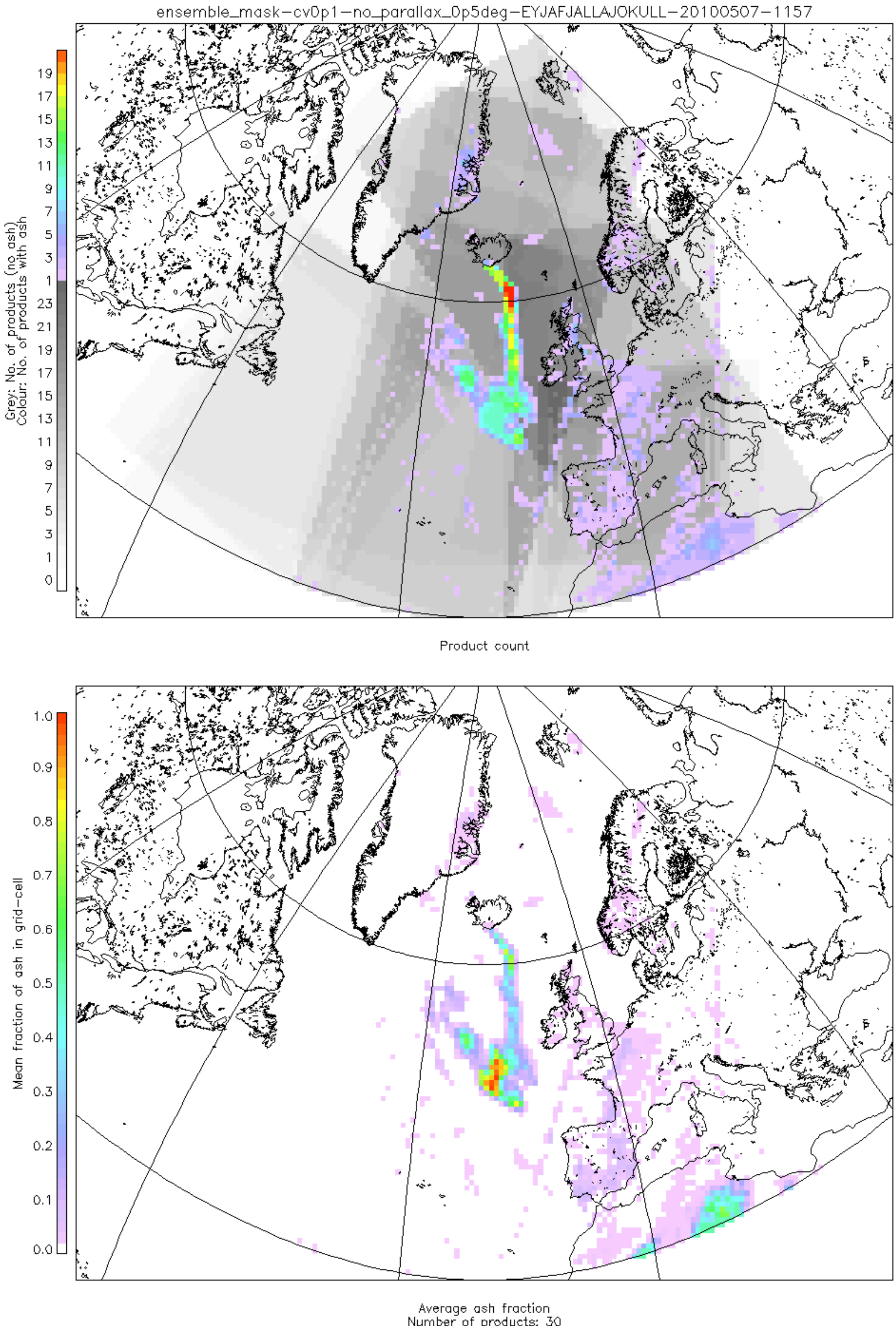

Figure 8: Ensemble ash mask for the Eyjafjallajkull eruption at approximately midday, 7 May 2010.

4.4 COMPARISON WITH LIDAR CURTAIN PLOTS

Again, using matches defined from the 0.5° gridded products, so-called curtain plots are created for each CALIOP and FAAM lidar matchup, as shown in Figure 9 and Figure 10 respectively. These plots provide a detailed view of a product in the region sampled by the lidar and are generated directly from the original product files (not from the regridded data). For each matchup the retrieved ash cloud-top height, collocated with the lidar track, is over-plotted on the lidar attenuated backscatter (from CALIOP) or extinction (from FAAM) profile along with its associated backscatter. In addition the satellite retrieval products in the region of the lidar measurements are also plotted. Due to the differences in the CALIOP and FAAM measurements, there are differences in how these plots are generated in each case:

- In the case of CALIOP, data was extracted along a 100 km wide swath, centred on the CALIPSO track and the following products were displayed (if available):
    - The 11-12 µm brightness temperature difference
    - The ash detection mask
    - The ash cloud-top height
    - The ash optical depth at 10 µm and 550 nm
    - The ash effective radius
    - The ash column mass density
    - In addition, the 8.7, 11 and 12 µm false-colour image provided by the Imaging Infrared Radiometer (IIR) on board CALIPSO is also plotted.
- In the case of FAAM, the aircraft track was broken into 15-minute segments, which were matched against the satellite products individually. Satellite data in a region centred on the FAAM track, with a 2 degree lat-lon margin[*], is plotted with the FAAM measurements over-plotted:
    - The ash detection mask, plotted on a map to provide geolocation for the scene
    - 11-12 µm brightness temperature difference (with FAAM ash detection over-plotted)
    - The ash cloud-top height (with the FAAM cloud-top height estimate over-plotted)
    - The ash optical depth at 10 µm and 550 nm (with the 550 nm optical depth estimated from the FAAM extinction over-plotted)
    - The ash effective radius (with FAAM ash detection over-plotted)
    - The ash column mass density (with mass density estimated from the FAAM extinction over-plotted)

  Note that, aside from the ash detection mask plot, all of the satellite imagery is plotted on the native grid supplied by the data product itself, which can result in differing orientations between scenes between products (even those from the same instrument).

[*] Note that, unlike the CALIPSO orbit track, the FAAM tracks contain frequent changes of direction and sampling as the aircraft changed direction, speed and altitude.

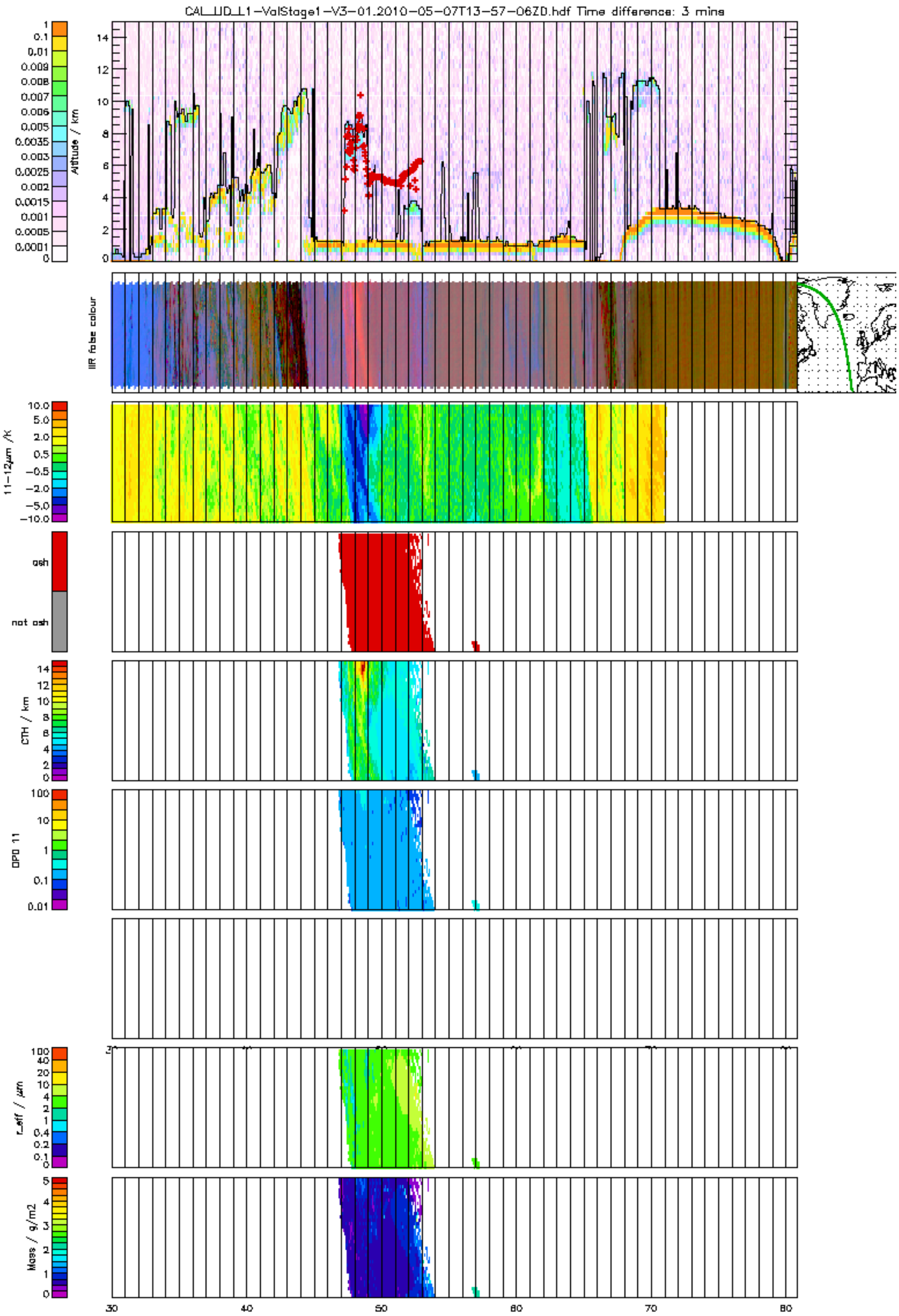

Figure 9: CALIOP curtain plot comparison of the NOAA SEVIRI product for the Eyjafjallajökull eruption at 14:30, 7 May 2010. Below the attenuated backscatter curtain plot the 8.7, 11, 12 µm false colour imagery from the IIR imager, the 11-12 µm BTD from SEVIRI, the NOAA SEVIRI ash mask, ash cloud-top height, 11 µm optical depth, a place holder for the missing 550 nm optical depth, ash effective radius and column mass loading.

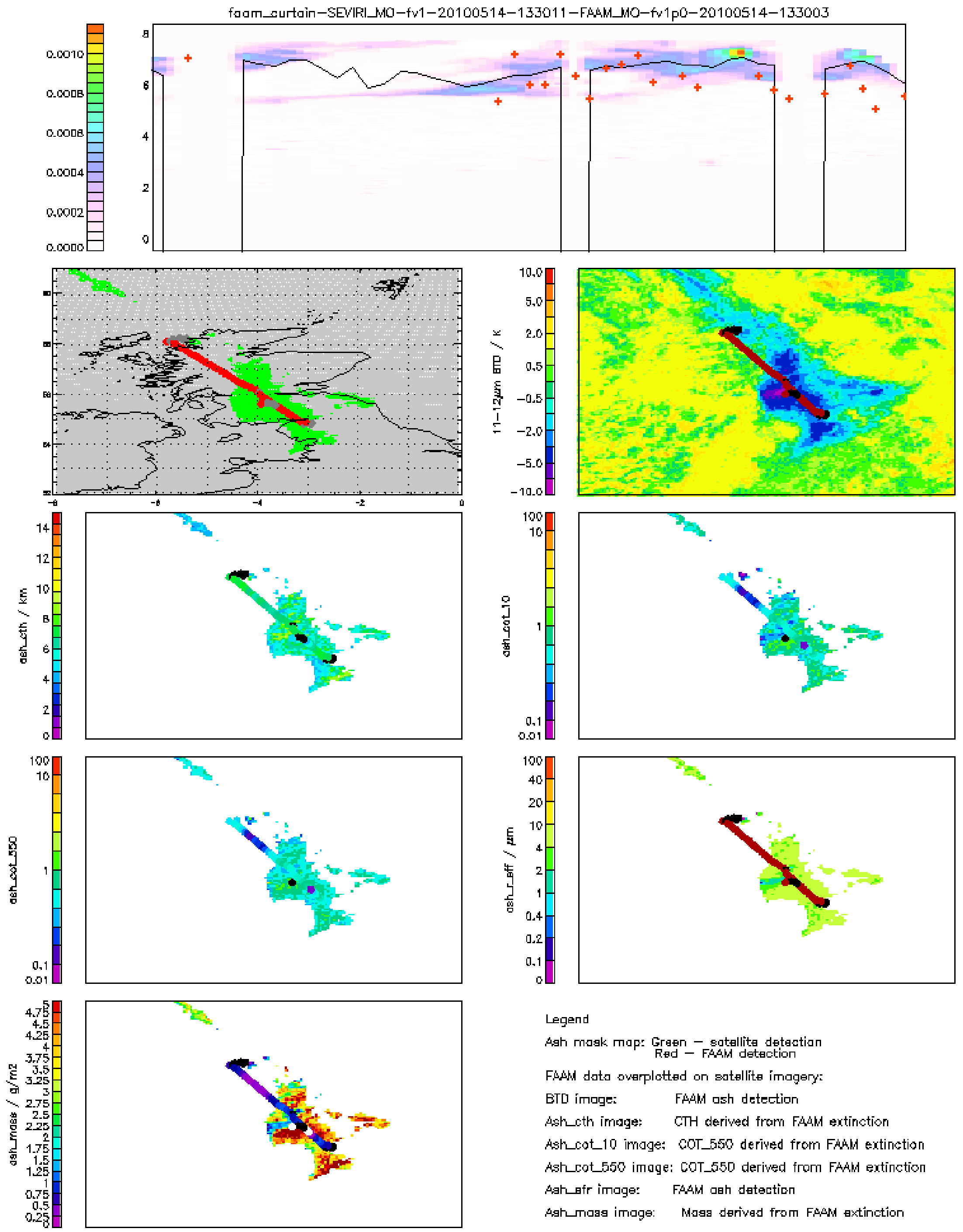

Figure 10: FAAM curtain comparison of the Met Office SEVIRI product for Eyjafjallajökull at 13:30, 14 April 2010. In the top curtain plot, the red crosses are CTH from the satellite retrieval and the black line is height derived from the FAAM measurements. Below the extinction curtain plot are (left-right, top-bottom): a map of the SEVIRI ash mask and imagery for the 11-12 µm BTD, ash cloud-top height, 11 µm optical depth, 550 nm optical depth, effective radius and column mass density. In each case the FAAM measurements are over-plotted, either with the equivalent data (where available) or with a simple measurement flag.

4.5 COMPARISON WITH DLR-FALCON MEASURMENTS

Twelve lidar measurements from the DLR Falcon aircraft made during the 2010 Eyjafjallajökull eruption were available for comparison, as summarised in Table 7. These data have been compared with each satellite product, using their native resolution. Matches were defined by:

- If the aircraft measurement time lies within the range defined by the time coverage attributes in the satellite product files.
- If the aircraft location lies within the range defined by the geospatial coverage attributes in the satellite product files, then the nearest pixel to the aircraft location within the scene is compared.

Note that not all the Falcon data points are from days that correspond with scenes selected for analysis in this study. The matches that are generated from the above criteria are summarised in Appendix A.1.

Date/time	Lat	Lon	Ash-cloud top height (km)	Ash-cloud base height (km)	Ash mass (gm^{-2})
2010-04-19 15:12:00	51.29	12.45	5.6	3.9	0.0425
2010-04-19 17:20:00	48.58	9.63	3.8	3.5	0.0048
2010-04-19 17:42:00	47.89	11.09	4.2	3.9	0.0051
2010-04-22 19:12:00	58.05	8.57	5.5	0.7	0.0768
2010-04-23 12:37:00	54.66	16.52	3.4	2.1	0.0247
2010-05-02 15:13:00	60.17	-15:17	3.7	1.6	0.4599
2010-05-09 14:58:00	48.38	12.60	4.9	3.5	0.0154
2010-05-13 14:13:00	53.41	1.45	5.4	2.8	0.0312
2010-05-16 14:11:00	54.76	-0.17	7.0	3.6	0.0714
2010-05-17 15:53:00	52.83	2.92	6.3	3.2	0.5766
2010-05-18 09:26:00	53.17	9.12	3.4	2.8	0.0324
2010-05-18 10:14:00	48.87	9.97	5.7	4.0	0.0340

Table 7: DLR-Falcon ash measurements

4.6 PAIR-WISE COMPARISON AT INSTRUMENT RESOLUTION

Finally, the 0.5° degree matched data were used as the basis to produce matches at close to the full instrument resolution, using the same methodology as described in point 2 above, but limiting matches to ±10 minutes. Each match-up was performed at the spatial resolution of the lowest resolution instrument in the pair, so that instrument resolution comparisons actually comprise a hierarchy of resolutions:

- If a match included the EUMETSAT PMAP product – which is on the GOME-2 instrument grid – then the native GOME-2 grid was used (rectangular scenes on the ground).
- If PMAP wasn't included, but an IASI product was, then the native IASI grid was used (12 km circular FOV on the ground).
- If neither of the above instruments were included, but a geostationary imager product (from either SEVIRI or MTSAT-1R or -2), then the appropriate geostationary grid is used (e.g. 3 km resolution at nadir for SEVIRI).

- If two different polar orbiting imagers (e.g. AATSR, AVHRR, MISR or MODIS) – or one of these instruments and an active sensor – formed the match, an approximately 4 km sinusoidal grid was used.
- If two products from the same polar orbiting imager formed the match, an approximately 1 km sinusoidal grid was used.

Note that the two final resolutions do not correspond directly to the measurement grids of the instruments involved. The 4 km sinusoidal grid was chosen for comparison of different polar imagers as it should minimise the sampling differences between the different instruments, while still provide reasonable spatial resolution. For comparing products from the same polar imager, a 1 km sinusoidal grid will ensure that individual instrument pixels are compared for the instruments included in the study, while allowing common gridding and mapping software to be used.

The plots produced from the instrument resolution comparisons mirrored those described in section 4.2, as shown in Figure 11, including the summary plots and statistics tables. In addition to the comparisons using the geolocation information provided by each product, the analysis has also been performed on parallax corrected data for imager data (unless comparing observations from the same platform), using the retrieved ash cloud-top height and instrument viewing geometry to calculate the nominal position of the ash if it were viewed vertically.

Note that generation of parallax corrected comparisons was complicated by the lack of pixel specific time and/or sub-satellite location in the data specification – this prevented the spectrometer products (PMAP and IASI products) from having parallax correction applied, as the viewing geometry could not be uniquely determined from the data products[†]. These parameters should be included future similar studies.

[†] In the case of imager based products, the satellite location is either fixed (for geostationary products) or can be assumed to lie at the centre of the imager swath.

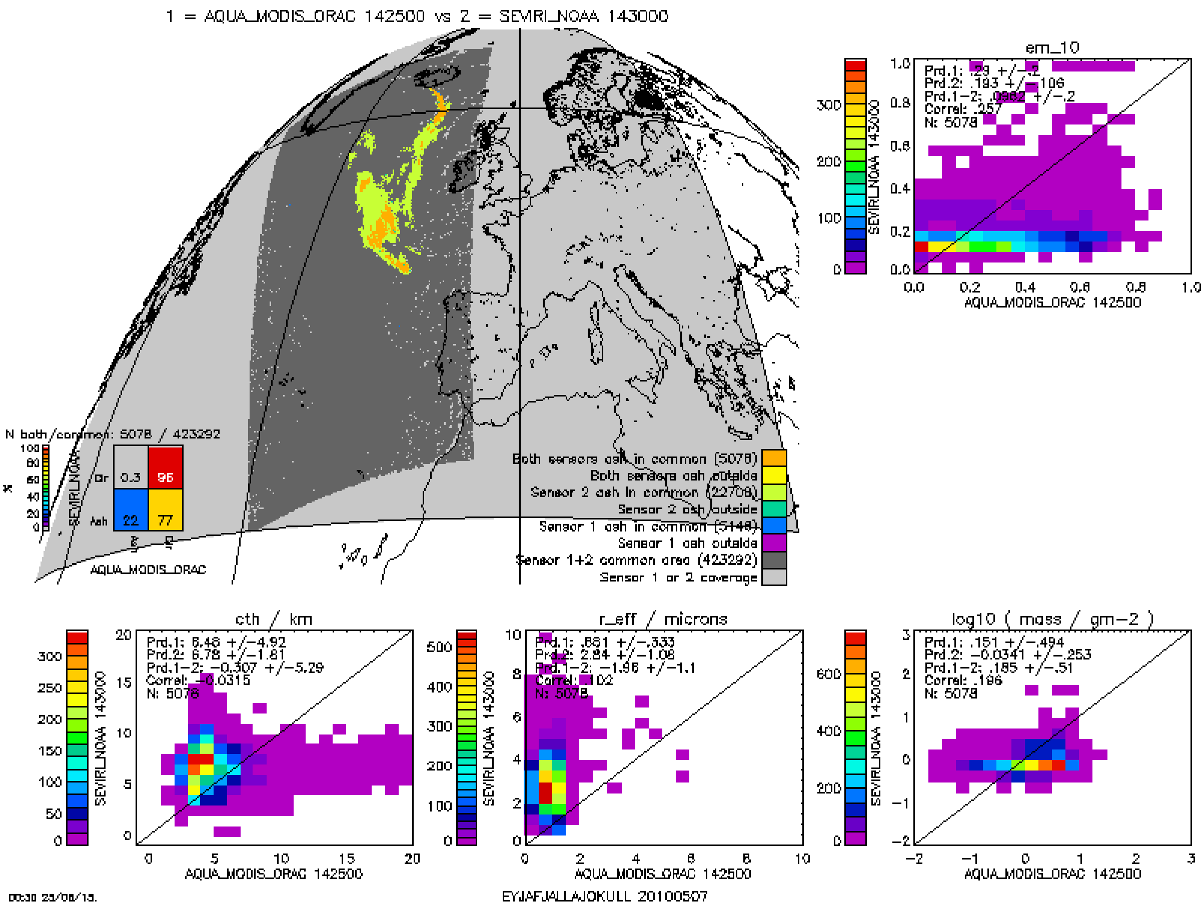

Figure 11: Instrument resolution (SEVIRI-pixel) comparison of MODIS-Aqua ORAC product from the University of Oxford and the SEVIRI product from NOAA at 14:30, 7 May 2010. This can be compared to the 0.5° grid plot shown in Figure 3. Note also that the NOAA product does not provide an ash optical depth at 550 nm, so the corresponding plot is missing.

5 EXPERT SCENE ANALYSIS

In a significant change from the 2015 study, to total of 11 scenes from Himawari-8 AHI and 50 scenes from SEVIRI have been analysed by hand by two separate experts (products HIMAWARI8_MANUAL1 and SEVIRI_MANUAL1 from the first expert, and HIMAWARI8_MANUAL2 and SEVIRI_MANUAL2 from the second). In the 2015 study, only a single manually classified scene was available and was handled separately in the analysis (this product, called SEVIRI_VOLCAT, remains in the standard analysis); in this study the manual scenes are treated in the same way as all of the other satellite products and is included in the standard analysis carried out on them. When viewing summary plots and other results, the special nature of these products should be kept in mind.

6 COMPARISON WITH ACTIVE SENSORS AND GEOMETRIC HEIGHT DETERMINATION

Excluding the limited DLR falcon dataset discussed in Section 4.5, two active sensor datasets were available for this study, as well as one well established geometrical height retrieval scheme. These data are essentially unchanged from the previous SCOPE comparison study – the initial plan included a substantially larger DLR dataset, which was not provided in time to be included in this work, and a new MISR dataset, which was not included in the intercomparison due to significant deviations from the required data format. The datasets used were:

1. The CALIOP lidar on board the CALIPSO satellite in the A-train. Level 1b attenuated backscatter profiles were compared against, using the same methodology as previous studies (Thomas and Siddans, 2015 and references within). The use of attenuated backscatter, rather than higher-level CALIOP aerosol and cloud products, ensures that the CALIOP data is free from its own retrieval artefacts.
2. The Leosphere ALS450 lidar system on board the NERC FAAM aircraft. Ash extinction profiles of Eyjafjallajökull ash over the UK, derived by the UK Met Office, were compared, using a similar methodology to that used for the CALIOP backscatter data.
3. The MISR stereo ash height retrieval from JPL. The multi-view parallax-based height estimation provided by MISR is expected to provide a more robust height estimate than the thermal emission-based methods used in most of the other passively sensed products in this study[‡].

The previous study also included results from the European EARLINET ground based lidar network. However, there were so few match-ups between these data and the satellite products, this was not pursed further in this study.

These products provide the closest data available to "ground-truth" on ash cloud height for this study. In practice, the vast majority of the matchups between the passively sensed data and the validation data occur with CALIOP, which is the only one of the above products that provides global data, and even this is quite sparse. Scatter plots of ash cloud-top height verses each of the validation products are shown for each of the eruption cases in Figure 12, Figure 13, Figure 14 and Figure 15 respectively, while summary statistics are given in Table 8 to Table 11.

[‡] The study also contains a stereo ash height retrieval from FMI using the AATSR instrument, carried over from the previous study. However, this product is still considered to be at a relatively early stage of development and has thus not been treated as a validation product.

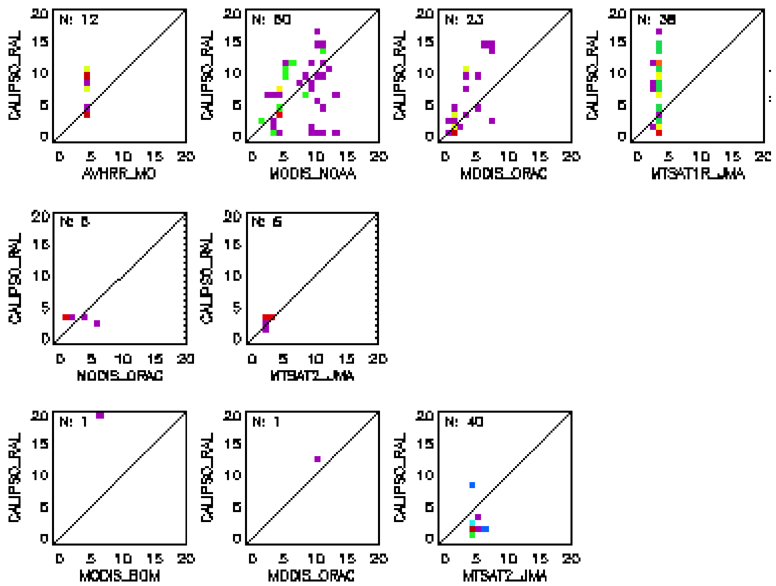

Figure 12: Scatter plots of retrieved ash cloud-top height against estimated height from the CALIOP lidar for the Sarychev (1st row), Kirishimayama (2nd row) and Kelut (3rd row) eruptions.

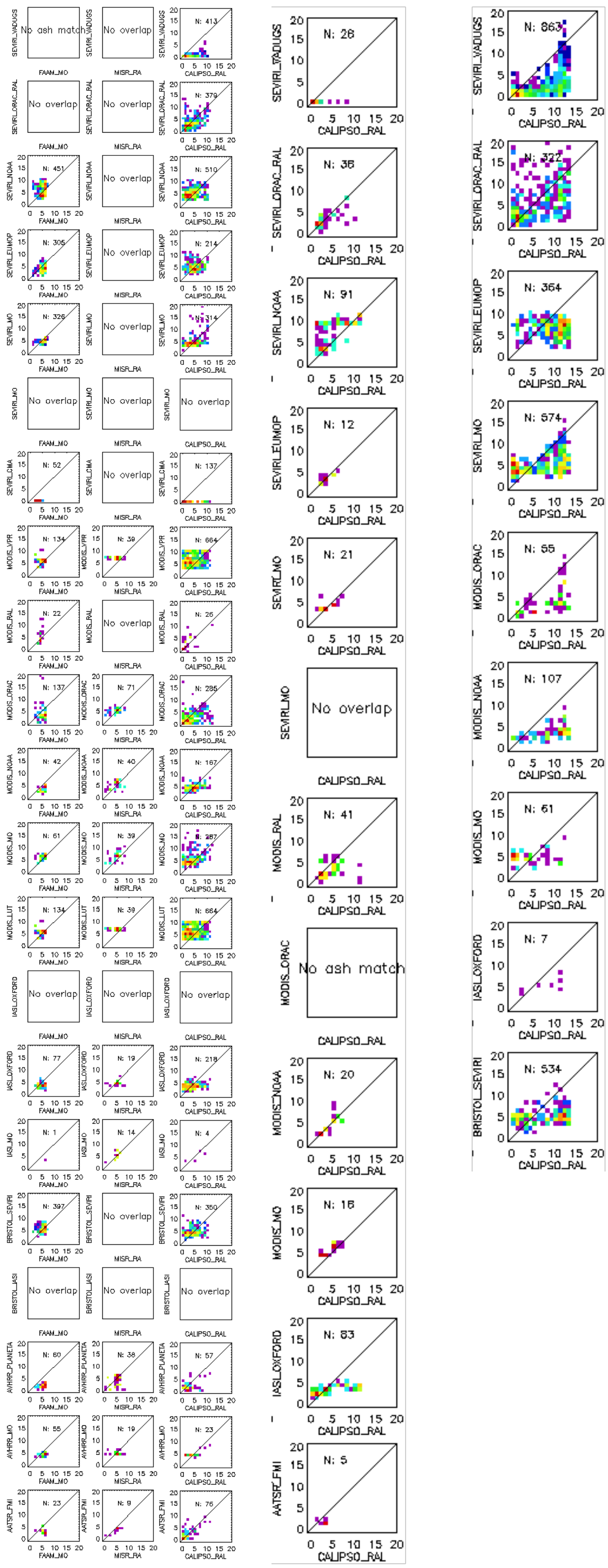

Figure 13: Scatter plots of retrieved ash cloud-top height against estimated height from the four validation datasets.

The first three columns show results for the Eyjafjallajökull eruption; from left to right: FAAM aircraft lidar, MISR stereo height, CALIOP orbital lidar.

The fourth and fifth columns show results for the Grimsvötn and Puyehue eruptions, respectively, where the CALIOP lidar is the only validation dataset available.

One aspect of these comparisons, which makes evaluation of the products difficult, is the paucity of matches for many of the instruments. This is particularly true for the FAAM measurements due to the limited coverage (both temporal and spatial). In the case of comparison and CALIOP, the density of matches depends strongly on the instrument being compared. For the geostationary platforms (where we have continuous coverage) and the MODIS instrument (MODIS-Aqua is part of the A-train formation along with CALIPSO), a large number of collocated pixels are available; for MetOp or ENVISAT based instruments far fewer matches are available. Finally, it should be noted that aside from the CALIOP product, all of the height validation data is specific to the Eyjafjallajökull eruption.

In general, simpler schemes tend to provide lower height correlations than more ambitious schemes, but show very little difference in RMS and mean/standard deviation difference; for instance the MODIS_LUT, MODIS_VPR and SEVIRI_EUMOP schemes versus the NOAA and ORAC based products. This can be attributed to the simpler schemes providing more self-consistent results – i.e. a fairly constant height is often retrieved across an individual image of a given cloud – but are more likely to produce spurious results. The more complex schemes, which apply a more comprehensive forward model to match the observations, are more robust, but provide much noisier results.

It is also obvious from the CALIOP comparisons in Figure 13 and Figure 15 (for the Eyjafjallajökull and Puyehue eruptions; the two which provide the most collocations) that the quality of retrieved ash height (and, by inference, the other retrieved parameters) varies from eruption to eruption. For example, the SEVIRI_NOAA ash cloud-top height product provides a correlation approaching 0.6 when compared against CALIOP for the Eyjafjallajökull eruption, which drops to under 0.4 for the Puyehue eruption. A similar pattern is seen for the other products which provide results from both eruptions. Although some of this difference could be due to the large areas of optically thin ash associated with the Puyehue eruption, it is also probably a reflection of the focus on Eyjafjallajökull in the development and characterisation of most satellite ash retrieval schemes and differences in the optical properties of the ash from the two eruptions.

The relatively small size of the eruptions for which the Himawari-AHI instrument provide data mean that there is a paucity of CALIOP data for these cases. Thus, no real conclusion can be drawn from the resulting statistics.

A final point worth noting is that the CALIOP ash retrieval product does not show very good agreement with the simple height estimate derived from the attenuated backscatter used as a reference here. This shows the danger involved in assuming active sensors provide an unambiguous, accurate measurement. In this case, the CALIOP ash product is providing the location of ash where its retrieval scheme is able to identify ash, and thus is likely to be biased to denser ash clouds.

Product	No. of matches	Correlation	Mean difference (km)	St. Dev. difference (km)	RMS (km)
AATSR_FMI	81	0.643	0.077	1.844	1.834
AHI_MO	10	-0.805	-3.940	0.924	4.036
AVHRR_MO	35	0.392	0.897	2.829	2.929
AVHRR_PLANETA	57	0.263	1.000	2.647	2.807
BRISTOL_SEVIRI	705	0.205	1.163	4.074	4.234
CALIOP	437	0.246	-3.176	3.945	5.061
HIMAWARI8_MSNZ	9	-0.258	-4.089	0.540	4.120
HIMAWARI8_NOAA	11	0.604	-3.418	0.623	3.469
IASI_MO	4	0.778	0.450	2.452	2.170
IASI_OXFORD	308	0.348	0.710	2.875	2.957
MODIS_BOM	1	-	13.600	-	-
MODIS_CENIZARG	25	0.00	8.952	4.939	10.176
MODIS_LUT	664	0.168	-2.307	3.225	3.963
MODIS_MO	366	0.298	-1.528	3.086	3.440
MODIS_NOAA	334	0.179	1.877	3.991	4.405
MODIS_ORAC	369	0.449	1.643	3.395	3.768
MODIS_RAL	66	0.269	0.633	3.056	3.098
MODIS_VPR	664	0.169	-2.303	3.223	3.959
SEVIRI_CMA	137	0.000	3.693	3.076	4.799
SEVIRI_EUMOP	590	0.147	1.456	3.978	4.233
SEVIRI_MO	905	0.392	0.867	4.013	4.104
SEVIRI_NOAA	601	0.350	-1.037	2.775	2.960
SEVIRI_ORAC_RAL	729	0.511	0.449	3.607	3.632
SEVIRI_VADUGS	1303	0.635	3.214	3.298	4.604

Table 8: Overall statistics of ash cloud-top height comparisons with the CALIOP lidar.

Product	No. of matches	Correlation	Mean difference (km)	St. Dev. difference (km)	RMS (km)
AATSR_FMI	23	-0.295	2.678	1.561	3.083
AVHRR_MO	55	0.255	1.520	0.985	1.806
AVHRR_PLANETA	60	0.342	3.563	1.120	3.732
BRISTOL_SEVIRI	370	0.416	-0.065	1.251	1.251
IASI_MO	1	-	3.200	-	-
IASI_OXFORD	77	0.011	1.234	1.515	1.946
MODIS_LUT	134	0.026	-0.563	1.747	1.829
MODIS_MO	61	0.637	-0.646	0.933	1.129
MODIS_NOAA	42	0.574	1.676	1.037	1.964
MODIS_ORAC	131	0.015	1.664	2.749	3.204

MODIS_RAL	22	0.523	-1.145	2.563	2.754
MODIS_VPR	134	0.027	-0.563	1.746	1.828
SEVIRI_CMA	52	0.000	3.442	0.909	3.558
SEVIRI_EUMOP	305	0.250	1.196	1.495	1.913
SEVIRI_MO	326	0.617	0.640	0.839	1.054
SEVIRI_NOAA	451	0.228	-0.448	2.193	2.236

Table 9: Overall statistics of ash cloud-top height comparisons with FAAM aircraft measurements.

7 SUMMARY OF CATANIA WORKSHOP

The workshop associated with this project was held at INGV in Catania, Italy over 8-12 October 2018. During the workshop the results of the intercomparison were presented, along with talks from representatives of several VAACs and satellite data providers. A summary of points to come from the workshop follows:

- Since 2015 there has been a significant growth in the use of satellite data by the VAACs, and an associated improvement in their understanding of the strengths and limitations of such products. This is particularly true of the North American VAACs, where NOAA has invested a lot of effort in improving the products supplied to VAACs, and the Asia-Pacific region, where Himawari has greatly improved the available data. Indeed, both the Darwin and Wellington VAAC noted that they have noticed a significant increase in the number of eruptions detected at all since the Himawari data has become available.
- The NOAA VOLCAT algorithm remains the most mature algorithm, largely due to the ash detection algorithms employed. The algorithm makes use of temporal and spatial constraints, in conjunction with the high spatial and temporal resolution of the new generation geostationary sensors, to provide a highly sensitive detection, while providing a very low false-detection rate. It should be noted that although several data providers use implementations of the VOLCAT algorithm, currently only the NOAA product utilises its full capabilities.
- The problem of validating satellite volcanic ash products, with the possible exception of height, was acknowledged as a continuing problem. It had been hoped that ash retrievals from the CALIOP instrument would provide a reliable ash detection and optical depth, but due to the small sample of products provided, their impact was limited.
- There was some debate centred on the manually classified products. In any future studies it was felt that manually classified scenes should be made available to data producers ahead of any intercomparison, so there is an opportunity for their use as a common ash mask. The lack of a common mask was a significant factor limiting the usefulness of comparisons of retrieved products in this study.

8 CONCLUDING REMARKS

This study has comprised the comparison of a large number of products, with varying spatial and temporal characteristics. Matching product pairs across all eruption cases has resulted in a large number of plots and summary statistics. Deriving firm conclusions from these results is very difficult, as:

- With the exception of the information on height provided by active sensors, and the expert classification ash mask for a single SEVIRI image, there is little ground truth with which to conduct a true validation.

- Different sensors, and even different products from the same sensor, provide different amounts of data in terms of coverage, spatial resolution and temporal coverage, which leads to strong sampling issues affecting comparisons of different product-pairs.
- Different products are available for each eruption case study.

Furthermore, when comparing ash detection between products, one is faced with the difficulty of what the goals each detection algorithm are. E.g. is the goal to identify "definite" ash pixels, the most likely total extent of the ash cloud, or those pixels suitable for ash property retrieval; all of these criteria will produce different ash detections and selecting the "best" becomes subjective. Furthermore, it is reasonable to assume that a retrieval scheme which aims to only provide results for "definite" ash pixels will, when all retrieved pixels are considered, provide more accurate derived properties (ash height, optical depth, etc) than schemes which include more complex, less clear-cut, pixels.

In the conclusions of the previous SCOPE ash inter-comparison, it was hoped that the inclusion of additional expert-classified ash scenes would provide a reliable common ash mask, which remove sampling biases in retrieved properties caused by differences in ash detection. This has not proved the case in the current study, for two reasons:

1. The manual classifications were not available early enough to provide a pre-defined ash mask for retrieval groups.
2. The manual classifications were not noticeably more conservative than the automated ash detection schemes used by the satellite products, and indeed indicated many pixels as containing ash which were not flagged as ash in most of the satellite products.

To allow a fully consistent comparison of ash retrieval products, a truly common and relatively conservative ash mask is a prerequisite.

The sub-setting of data in terms of land/sea and viewing geometry proved to provide limited additional information, except to confirm that automated ash detection routines are generally more reliable over the ocean than land (where false positive detections are far more likely). Unfortunately, due to constraints of staff availability, the proposed use of CALIPSO to identify pixels with and without associated meteorological clouds, and to sub-set the inter-comparison accordingly, was not carried out. This remains a recommendation for future studies.

In addition, the recommendations provided in the previous study remain relevant:

- Allowing more time for retrieval teams to produce a more complete set of results for inclusion in the inter-comparison.
- Adopting an iterative approach to the inter-comparison exercise, whereby retrieval teams can submit improved/more consistent products and the comparison approach can be refined, based on each revision of the exercise.
- Large scale comparisons such as presented here, could be complemented by focused case studies designed to reveal the reasons for differences between products:
  - Focus on some well understood test scenes.
  - Constrain common retrieval inputs (eg. Ash optical properties, ancillary data such as Met-fields).

Thus, the main qualitative conclusions which can be draw from this study are consistent with the previous work:

- The intervening three years between this study and the previous work have not seen a substantial improvement in the satellite derived ash products produced by most groups. (Note that this does not imply that there haven't been improvements in ash detection and retrieval by some schemes, or improvements in the use and understanding of satellite products in VAACs. Such improvements, particularly in the use of spatio-temporal information in the detection and tracking of ash, were evident at the ash retrieval workshop associated with this project).
- Height and mass tend to "validate"/inter-compare relatively well compared to optical depth and effective radius. This is likely a reflection of the limited knowledge of, and relatively simplistic treatment of, ash optical properties in the retrieval algorithms. This problem is undoubtedly complicated by the variability of ash properties from eruption-to-eruption (and even over the course of a single eruption).
- Most schemes perform well in some situations, though it is not always straightforward to focus the comparison on these (beyond drilling down to specific days/scenes). There is little consistency between products in which scenes provide the best results.
- Difficult to validate height for Puyehue without more careful identification of ash in CALIPSO
- The MODIS and SEVIRI schemes from NOAA show an overall high level of maturity:
    - Their ash detection, while not conservative (the extent of the detected ash cloud tends to be larger than in most other products and the expert identified SEVIRI scene), it not prone to the scattered false detection prevalent in many other products. This has only improved since the previous study.
    - They have good level of consistency with each other, and actively sensed data, for height and mass.
    - They also have tendency to correlate with other schemes (less so for optical depth). This is likely at least partially due to the removal of false-positives from other products by the co-location criteria with the NOAA ash mask.
    - These points also hold true for the NOAA Himawari-AHI product, although quantitative comparisons against actively sensed data are limited.
- IASI schemes seem to provide robust ash detection. Characterising the quality of optical depth, effective radius and mass are hampered by the relatively low spatial resolution of the instrument.
- Tendency for simpler schemes to produce more consistent results. More ambitious schemes sometimes work better but also prone noise and to deviate more in "difficult" conditions – suggesting a trade-off between robustness and extracting maximum information.

9 REFERENCES

RD-1. Thomas, G. E and R. Siddans, "Development of OCA type processors to volcanic ash detection and retrieval:", Final Report EUMETSAT Contract: EUM/C0/13/4600001276/PDW.

RD-2. Eumetsat, Satellite Derived Volcanic Ash Product Inter-Comparison in Support to SCOPE-Nowcasting, Statement of work EUM/TSS/SOW/14/778570, 28 October 2014

RD-3. WMO, SCOPE-Nowcasting Pilot Project 2 : Globally consistent Volcanic Ash Products, Meeting on the Intercomparison of Satellite-based Volcanic Ash Retrieval Algorithms, 2015, FINAL REPORT, http://www.wmo.int/pages/prog/sat/documents/SCOPE-NWC-PP2_VAIntercompWSReport2015.pdf

RD-4. Eumetsat, Follow-on to the Inter-comparison of Satellite-based Volcanic Ash Retrieval Algorithms in support of SCOPE-Nowcasting, Statement of work EUM/RSP/SOW/17/964405, 14 December 2017.

A APPENDICES

A.1 DLR FALCON MATCHES

The following table lists the satellite scenes which provided spatial and temporal matches with the DLR aircraft data, as described in Section 4.5. The table columns are as follows:

- Satellite product name.
- Start time of the satellite scene, as defined in the data file.
- Difference in latitude between the aircraft location and the nearest satellite pixel, defined as lat_{DLR} - lat_{Sat}.
- Difference in longitude, defined in the same way as latitude difference.
- Whether the satellite product flags ash at this location (with 1 indicating ash detection)
- The satellite derived ash cloud top height (CTH), if the satellite product has flagged ash (km).
- The difference between the aircraft and satellite derived ash cloud top height, if the satellite product has flagged ash. Again, defined as DLR-Sat.
- The satellite derived column ash mass, if ash has been flagged (gm^{-2}).
- The difference between the aircraft and satellite derived column ash mass. Again, defined as DLR-Sat.

Satellite Product	Scene start time	Δlat	Δlon	Ash flag	Sat CTH	ΔCTH	Sat ash mass	Δmass
AVHRR_MO	20100518T092400Z	-0.004	0.002	0	-	-	-	-
AVHRR_PLANETA	20100518T092303Z	0.000	-0.004	0	-	-	-	-
BRISTOL_SEVIRI	20100509T143000Z	0.017	0.021	0	-	-	-	-
BRISTOL_SEVIRI	20100509T144500Z	0.017	0.021	0	-	-	-	-
BRISTOL_SEVIRI	20100509T150000Z	0.017	0.021	0	-	-	-	-
BRISTOL_SEVIRI	20100509T151500Z	0.017	0.021	0	-	-	-	-
BRISTOL_SEVIRI	20100513T134500Z	-0.003	-0.001	0	-	-	-	-
BRISTOL_SEVIRI	20100513T140000Z	-0.003	-0.001	0	-	-	-	-
BRISTOL_SEVIRI	20100513T141500Z	-0.003	-0.001	0	-	-	-	-
BRISTOL_SEVIRI	20100513T143000Z	-0.003	-0.001	0	-	-	-	-
BRISTOL_SEVIRI	20100516T134500Z	-0.005	-0.020	0	-	-	-	-
BRISTOL_SEVIRI	20100516T140000Z	-0.005	-0.020	0	-	-	-	-

BRISTOL_SEVIRI	20100516T141500Z	-0.005	-0.020	0	-	-	-	-
BRISTOL_SEVIRI	20100516T143000Z	-0.005	-0.020	0	-	-	-	-
BRISTOL_SEVIRI	20100517T153000Z	0.002	0.012	1	4.478	1.822	0.583	-0.007
BRISTOL_SEVIRI	20100517T154500Z	0.002	0.012	1	4.478	1.822	0.517	0.059
BRISTOL_SEVIRI	20100517T160000Z	0.002	0.012	1	4.483	1.817	0.512	0.064
BRISTOL_SEVIRI	20100517T161500Z	0.002	0.012	1	4.478	1.822	0.518	0.059
BRISTOL_SEVIRI	20100518T090000Z	-0.010	-0.016	0	-	-	-	-
BRISTOL_SEVIRI	20100518T091500Z	-0.010	-0.016	0	-	-	-	-
BRISTOL_SEVIRI	20100518T093000Z	-0.010	-0.016	0	-	-	-	-
BRISTOL_SEVIRI	20100518T094500Z	-0.010	-0.016	0	-	-	-	-
BRISTOL_SEVIRI	20100518T094500Z	-0.025	0.005	0	-	-	-	-
BRISTOL_SEVIRI	20100518T100000Z	-0.025	0.005	0	-	-	-	-
BRISTOL_SEVIRI	20100518T101500Z	-0.025	0.005	0	-	-	-	-
BRISTOL_SEVIRI	20100518T103000Z	-0.025	0.005	0	-	-	-	-
IASI_MO	20100518T092400Z	-0.038	0.066	0	-	-	-	-
IASI_OXFORD	20100518T092355Z	-0.038	0.066	0	-	-	-	-
METOPA_PMA	20100518T092356Z	-0.071	0.062	0	-	-	-	-
MODIS_LUT	20100518T104000Z	0.003	-0.001	0	-	-	-	-
MODIS_MO	20100518T104000Z	0.003	-0.001	0	-	-	-	-
MODIS_VPR	20100518T104000Z	0.003	-0.001	0	-	-	-	-
SEVIRI_EUMOP	20100509T143000Z	0.018	-0.023	0	-	-	-	-
SEVIRI_EUMOP	20100509T144500Z	0.018	-0.023	0	-	-	-	-
SEVIRI_EUMOP	20100509T150000Z	0.018	-0.023	0	-	-	-	-
SEVIRI_EUMOP	20100509T151500Z	0.018	-0.023	0	-	-	-	-
SEVIRI_EUMOP	20100513T134500Z	0.000	-0.001	0	-	-	-	-
SEVIRI_EUMOP	20100513T140000Z	0.000	-0.001	0	-	-	-	-
SEVIRI_EUMOP	20100513T141500Z	0.000	-0.001	0	-	-	-	-
SEVIRI_EUMOP	20100513T143000Z	0.000	-0.001	0	-	-	-	-
SEVIRI_EUMOP	20100516T134500Z	-0.001	-0.020	0	-	-	-	-
SEVIRI_EUMOP	20100516T140000Z	-0.001	-0.020	0	-	-	-	-
SEVIRI_EUMOP	20100516T141500Z	-0.001	-0.020	0	-	-	-	-
SEVIRI_EUMOP	20100516T143000Z	-0.001	-0.020	0	-	-	-	-
SEVIRI_EUMOP	20100517T153000Z	0.005	0.012	1	3.079	3.221	6.538	-5.961
SEVIRI_EUMOP	20100517T154500Z	0.005	0.012	1	3.726	2.574	3.648	-3.071
SEVIRI_EUMOP	20100517T160000Z	0.005	0.012	1	3.702	2.598	3.622	-3.045
SEVIRI_EUMOP	20100517T161500Z	0.005	0.012	1	2.930	3.370	5.462	-4.885
SEVIRI_EUMOP	20100518T090000Z	-0.007	-0.016	0	-	-	-	-
SEVIRI_EUMOP	20100518T091500Z	-0.007	-0.016	0	-	-	-	-
SEVIRI_EUMOP	20100518T093000Z	-0.007	-0.016	0	-	-	-	-
SEVIRI_EUMOP	20100518T094500Z	-0.007	-0.016	0	-	-	-	-
SEVIRI_EUMOP	20100518T094500Z	-0.022	0.006	0	-	-	-	-
SEVIRI_EUMOP	20100518T100000Z	-0.022	0.006	0	-	-	-	-
SEVIRI_EUMOP	20100518T101500Z	-0.022	0.006	0	-	-	-	-
SEVIRI_EUMOP	20100518T103000Z	-0.022	0.006	0	-	-	-	-
SEVIRI_MO	20100509T143011Z	-0.010	-0.008	0	-	-	-	-
SEVIRI_MO	20100509T144511Z	-0.010	-0.008	0	-	-	-	-
SEVIRI_MO	20100509T150010Z	-0.010	-0.008	0	-	-	-	-
SEVIRI_MO	20100509T151510Z	-0.010	-0.008	0	-	-	-	-
SEVIRI_MO	20100513T134510Z	0.027	-0.024	0	-	-	-	-
SEVIRI_MO	20100513T140010Z	0.027	-0.024	0	-	-	-	-
SEVIRI_MO	20100513T141510Z	0.027	-0.024	0	-	-	-	-
SEVIRI_MO	20100513T143010Z	0.027	-0.024	0	-	-	-	-

SEVIRI_MO	20100516T134510Z	0.027	0.005	0	-	-	-	-
SEVIRI_MO	20100516T140010Z	0.027	0.005	0	-	-	-	-
SEVIRI_MO	20100516T141510Z	0.027	0.005	0	-	-	-	-
SEVIRI_MO	20100516T143010Z	0.027	0.005	0	-	-	-	-
SEVIRI_MO	20100517T153010Z	-0.028	-0.014	0	-	-	-	-
SEVIRI_MO	20100517T154511Z	-0.028	-0.014	0	-	-	-	-
SEVIRI_MO	20100517T160011Z	-0.028	-0.014	0	-	-	-	-
SEVIRI_MO	20100517T161510Z	-0.028	-0.014	0	-	-	-	-
SEVIRI_MO	20100518T090010Z	0.021	0.015	0	-	-	-	-
SEVIRI_MO	20100518T091510Z	0.021	0.015	0	-	-	-	-
SEVIRI_MO	20100518T093010Z	0.021	0.015	0	-	-	-	-
SEVIRI_MO	20100518T094510Z	0.021	0.015	0	-	-	-	-
SEVIRI_MO	20100518T094510Z	0.001	-0.011	0	-	-	-	-
SEVIRI_MO	20100518T100010Z	0.001	-0.011	0	-	-	-	-
SEVIRI_MO	20100518T101510Z	0.001	-0.011	0	-	-	-	-
SEVIRI_MO	20100518T103010Z	0.001	-0.011	0	-	-	-	-
SEVIRI_NOAA	20100509T143000Z	0.002	-0.004	0	-	-	-	-
SEVIRI_NOAA	20100509T144500Z	0.002	-0.004	0	-	-	-	-
SEVIRI_NOAA	20100509T150000Z	0.002	-0.004	0	-	-	-	-
SEVIRI_NOAA	20100509T151500Z	0.002	-0.004	0	-	-	-	-
SEVIRI_NOAA	20100516T134500Z	-0.022	0.005	0	-	-	-	-
SEVIRI_NOAA	20100516T140000Z	-0.022	0.005	0	-	-	-	-
SEVIRI_NOAA	20100516T141500Z	-0.022	0.005	0	-	-	-	-
SEVIRI_NOAA	20100516T143000Z	-0.022	0.005	1	6.309	0.691	1.831	-1.759
TERRA_MODIS_ORAC	20100518T104009Z	0.003	-0.001	0	-	-	-	-
AVHRR_MO	20100518T092400Z	-0.004	0.002	0	-	-	-	-
AVHRR_PLANETA	20100518T092303Z	0.000	-0.004	0	-	-	-	-
BRISTOL_SEVIRI	20100509T143000Z	0.017	0.021	0	-	-	-	-
BRISTOL_SEVIRI	20100509T144500Z	0.017	0.021	0	-	-	-	-
BRISTOL_SEVIRI	20100509T150000Z	0.017	0.021	0	-	-	-	-
BRISTOL_SEVIRI	20100509T151500Z	0.017	0.021	0	-	-	-	-
BRISTOL_SEVIRI	20100513T134500Z	-0.003	-0.001	0	-	-	-	-
BRISTOL_SEVIRI	20100513T140000Z	-0.003	-0.001	0	-	-	-	-
BRISTOL_SEVIRI	20100513T141500Z	-0.003	-0.001	0	-	-	-	-
BRISTOL_SEVIRI	20100513T143000Z	-0.003	-0.001	0	-	-	-	-
BRISTOL_SEVIRI	20100516T134500Z	-0.005	-0.020	0	-	-	-	-
BRISTOL_SEVIRI	20100516T140000Z	-0.005	-0.020	0	-	-	-	-
BRISTOL_SEVIRI	20100516T141500Z	-0.005	-0.020	0	-	-	-	-
BRISTOL_SEVIRI	20100516T143000Z	-0.005	-0.020	0	-	-	-	-
BRISTOL_SEVIRI	20100517T153000Z	0.002	0.012	1	4.478	1.822	0.583	-0.007
BRISTOL_SEVIRI	20100517T154500Z	0.002	0.012	1	4.478	1.822	0.517	0.059
BRISTOL_SEVIRI	20100517T160000Z	0.002	0.012	1	4.483	1.817	0.512	0.064
BRISTOL_SEVIRI	20100517T161500Z	0.002	0.012	1	4.478	1.822	0.518	0.059
BRISTOL_SEVIRI	20100518T090000Z	-0.010	-0.016	0	-	-	-	-
BRISTOL_SEVIRI	20100518T091500Z	-0.010	-0.016	0	-	-	-	-
BRISTOL_SEVIRI	20100518T093000Z	-0.010	-0.016	0	-	-	-	-